

See discussions, stats, and author profiles for this publication at: <https://www.researchgate.net/publication/222896946>

Paleozoic tectonism on the East Gondwana margin: Evidence from SHRIMP U-Pb zircon geochronology of a migmatite–granite complex in West Antarctica

Article in *Tectonophysics* · November 2009

DOI: 10.1016/j.tecto.2009.04.021

CITATIONS

47

READS

150

2 authors:



Christine S Siddoway

Colorado College

121 PUBLICATIONS 1,573 CITATIONS

[SEE PROFILE](#)



Christopher Mark Fanning

Australian National University

598 PUBLICATIONS 29,708 CITATIONS

[SEE PROFILE](#)

Some of the authors of this publication are also working on these related projects:

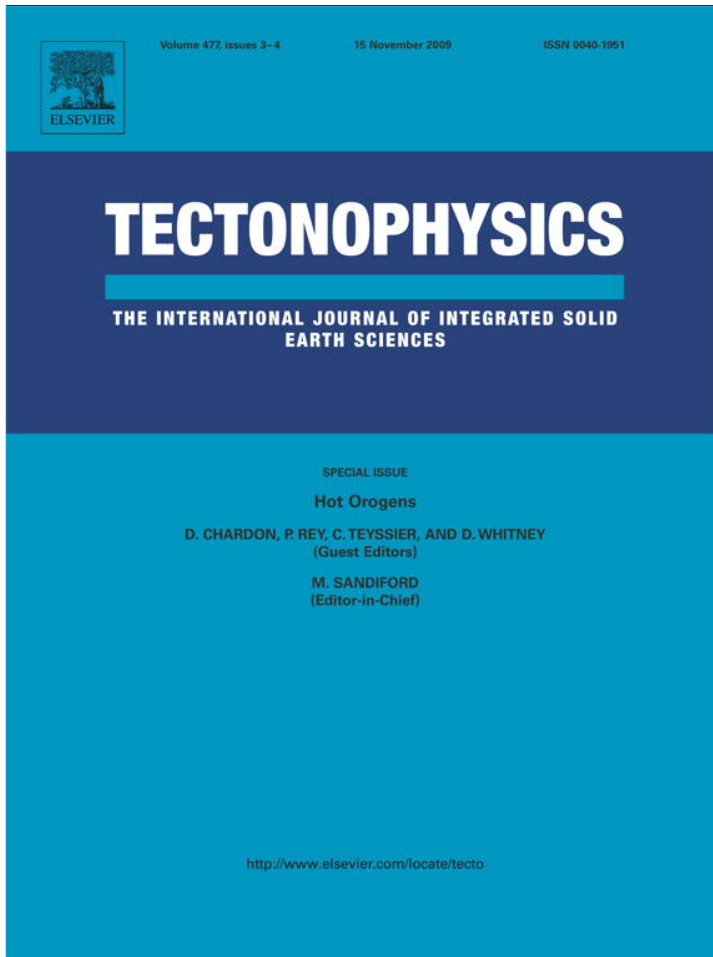


Tectonic development of the active margin of Gondwana in Antarctica [View project](#)



Pre late-Miocene tectonics along the Liquiñe-Ofqui Fault Zone [View project](#)

Provided for non-commercial research and education use.
Not for reproduction, distribution or commercial use.



This article appeared in a journal published by Elsevier. The attached copy is furnished to the author for internal non-commercial research and education use, including for instruction at the authors institution and sharing with colleagues.

Other uses, including reproduction and distribution, or selling or licensing copies, or posting to personal, institutional or third party websites are prohibited.

In most cases authors are permitted to post their version of the article (e.g. in Word or Tex form) to their personal website or institutional repository. Authors requiring further information regarding Elsevier's archiving and manuscript policies are encouraged to visit:

<http://www.elsevier.com/copyright>



Contents lists available at ScienceDirect

Tectonophysics

journal homepage: www.elsevier.com/locate/tecto

Paleozoic tectonism on the East Gondwana margin: Evidence from SHRIMP U–Pb zircon geochronology of a migmatite–granite complex in West Antarctica

Christine S. Siddoway ^{a,*}, C. Mark Fanning ^b^a Department of Geology, The Colorado College, Colorado Springs, Colorado 80903, USA^b Research School of Earth Sciences, The Australian National University, Mills Road, Canberra ACT 0200, Australia

ARTICLE INFO

Article history:

Received 23 November 2008

Received in revised form 6 April 2009

Accepted 19 April 2009

Available online 23 April 2009

Keywords:

East Gondwana

Accretionary orogen

West Antarctica

SHRIMP U–Pb zircon geochronology

Migmatite–granite complex

ABSTRACT

The Fosdick Mountains migmatite–granite complex in West Antarctica records episodes of crustal melting and plutonism in Devonian–Carboniferous time that acted to transform transitional crust, dominated by immature oceanic turbidites of the accretionary margin of East Gondwana, into stable continental crust. West Antarctica, New Zealand and Australia originated as contiguous parts of this margin, according to plate reconstructions, however, detailed correlations are uncertain due to a lack of isotopic and geochronological data. Our study of the mid-crustal exposures of the Fosdick range uses U–Pb SHRIMP zircon geochronology to examine the tectonic environment and timing for Paleozoic magmatism in West Antarctica, and to assess a correlation with the better known Lachlan Orogen of eastern Australia and Western Province of New Zealand. NNE–SSW to NE–SW contraction occurred in West Antarctica in early Paleozoic time, and is expressed by km-scale folds developed both in lower crustal metasedimentary migmatite gneisses of the Fosdick Mountains and in low greenschist-grade turbidite successions of the upper crust, present in neighboring ranges. The metasedimentary rocks and structures were intruded by calc-alkaline, I-type plutons attributed to arc magmatism along the convergent East Gondwana margin. Within the Fosdick Mountains, the intrusions form a layered plutonic complex at lower structural levels and discrete plutons at upper levels. Dilatational structures that host anatexic granite overprint plutonic layering and migmatitic foliation. They exhibit systematic geometries indicative of NNE–SSW stretching, parallel to a first-generation mineral lineation. New U–Pb SHRIMP zircon ages for granodiorite and porphyritic monzogranite plutons, and for leucogranites that occupy shear bands and other mesoscopic-scale structural sites, define an interval of 370 to 355 Ma for plutonism and migmatization.

Paleozoic plutonism in West Antarctica postdates magmatism in the western Lachlan Orogen of Australia, but it coincides with that in the central part of the Lachlan Orogen and with the rapid main phase of emplacement of the Karamea Batholith of the Western Province, New Zealand. Emplaced within a 15 to 20 million year interval, the Paleozoic granitoids of the Fosdick Mountains are a product of subduction-related plutonism associated with high temperature metamorphism and crustal melting. The presence of anatexic granites within extensional structures is a possible indication of alternating strain states ('tectonic switching') in a supra-subduction zone setting characterized by thin crust and high heat flow along the Devonian–Carboniferous accretionary margin of East Gondwana.

© 2009 Elsevier B.V. All rights reserved.

1. Introduction

Since the recognition of circum-Pacific-style accretionary margin orogens formed within voluminous turbidite systems supported by oceanic crust (Coney, 1992; Fergusson and Coney, 1992), there has been a growth in understanding of the role that metamorphism, crustal melting, and magmatism played in the transformation and stabilization of the wide active margin of East Gondwana (Fig. 1).

In addition to subduction-related magmatism (Muir et al., 1996; Pankhurst et al., 1998; Jenkins et al., 2002) and medium to high

pressure metamorphism induced by crustal thickening (Ireland and Gibson, 1998; Spaggiari et al., 2002), felsic magmatism and high temperature (HT) metamorphism also occurred, as a consequence of rapid extension within the overriding Gondwana plate. Heat and magmas derived from the mantle caused voluminous melting in areas of thin crust in the Lachlan Belt of Australia (Collins, 2002; Kemp et al., 2007) and in New Zealand (Tulloch et al., 2009), where short-lived intra-arc and back-arc extension caused dramatic thinning of the lithosphere and brought hot asthenosphere into proximity with the crust (Collins, 2002). Recent isotope studies document a high degree of interaction of mantle-derived magmas with metasedimentary crust (Hawkesworth and Kemp, 2006; Kemp et al., 2007) that led to formation of the classic calc-alkaline I-type plutonic rocks in Australia

* Corresponding author. Tel.: +1 719 389 6717; fax: +1 719 389 6910.
E-mail address: csiddoway@coloradocollege.edu (C.S. Siddoway).

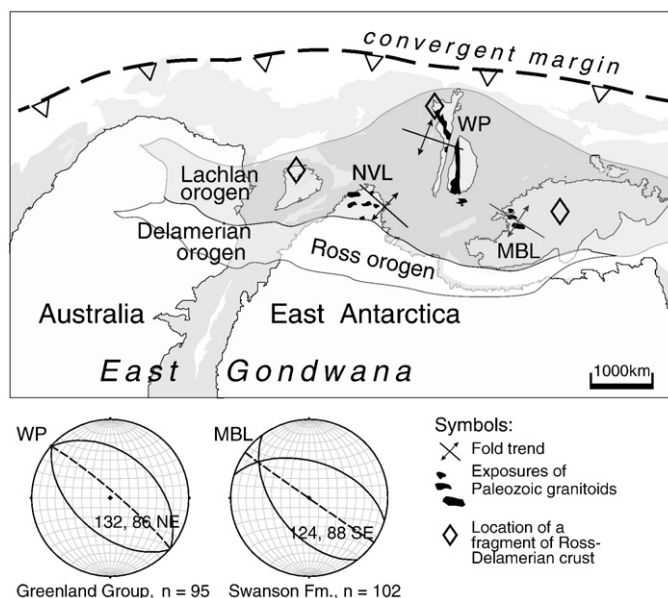


Fig. 1. Schematic reconstruction of the Paleozoic margin of East Gondwana, showing the position of the Delamerian–Ross orogen and the accretionary belt (grey) developed outboard of it. In the accretionary belt, lower Paleozoic metasedimentary rocks originated as detritus shed from the Delamerian–Ross mountains, then experienced contraction recorded by km-scale open, upright, symmetrical folds in Marie Byrd Land (MBL) and north Victoria Land (NVL), Antarctica, and the Western Province (WP) of New Zealand. Stereographic diagrams depict the mean fold orientation (fold limbs and axes in present-day coordinates) for coastal exposures of the Greenland Group of New Zealand (Nathan et al., 2002) and for Swanson Formation in Marie Byrd Land (Siddoway, unpublished; J.D. Bradshaw, unpublished). The location of Ross–Delamerian crustal slivers (Bradshaw, 2007; Berry et al., 2008) is indicated with the diamond symbol.

(Chappell and White, 1992). Voluminous silicic magmatism of the Karamea Batholith in the Western Province, New Zealand, is also attributed to advection of heat and magma derived from mantle, with rapid melting of metasedimentary crust, during one such extension phase (Tulloch et al., 2009).

The contemporary view is that East Gondwana plutonism occurred in an immense back-arc province comprising voluminous turbidite fan deposits accumulated upon primitive crust (Fergusson and Coney, 1992; Glen, 2005) inboard of a longstanding convergent margin (Foster and Gray, 2000; Collins and Hobbs, 2001; Spaggiari et al., 2002, 2003; Gray and Foster, 2004). The prevalent record of contraction and folding of the thick sequences of immature sedimentary rocks is punctuated by episodes of extension and extreme crustal thinning, with HT metamorphism, crustal melting, and magmatism (Gray et al., 1997; Gray and Foster, 1998; Foster et al., 1999; Foster and Gray, 2000; Collins, 2002). The recognition that a distinctive style of ‘hot orogen’ may develop upon accretionary tectonic margins leads to the following questions: What was the original lateral extent of the Lachlan-type orogen? What is the duration of orogenic phases and over what time frames do associated plutonism and crustal melting occur? Does the deep crust preserve a record of cycles of extensional deformation corresponding to those found in the upper crust?

New perspective on these questions comes from the Ross Province in West Antarctica (Pankhurst et al., 1998; Bradshaw, 2007), where calc-alkaline, I-type Ford Granodiorite equated with a convergent margin arc (Weaver et al., 1991) was emplaced at *circa* 375 to 353 Ma (Pankhurst et al., 1998). The granodiorite is hosted by metaturbidites that are widespread within once-contiguous parts of the East Gondwana margin in Australia and New Zealand (Fig. 1) (Ireland et al., 1998; Adams, 2004; Bradshaw, 2007; Tulloch et al., 2009). Valuable new geological and geochronological information for West Antarctica comes from the Fosdick Mountains (Fig. 2), an exposure of middle crust that contains a record of Devonian–Carboniferous plutonism (Siddoway et al., 2006; Saito et al., 2007a) and HT metamorphism (Korhonen et al., 2007) that initiated during tectonic convergence and continued into a post-orogenic phase of tectonism (cf. Pankhurst et al., 1998). In this paper, we present aspects of the Paleozoic deformation history together with new U–Pb zircon geochronology acquired by SHRIMP (sensitive high

resolution ion microprobe) for eight granitoid samples. The data provide insights into whether Paleozoic plutonism was synchronous along the full length of East Gondwana’s convergent margin and whether there was along-strike continuity of lithospheric elements that influenced the degree of heating and melt productivity along the active margin.

2. Geological background

Quartzose turbidite and flysch sequences of Lachlan type represent detritus eroded from and accumulated outboard of the Cambrian Delamerian–Ross Orogen (Flöttmann et al., 1993; Ireland et al., 1998; Adams, 2004) in Australia and in once-contiguous sectors of New Zealand and Marie Byrd Land (MBL), Antarctica (Fig. 1). Folding and low grade metamorphism broadly affected the margin in the Late Ordovician between 450 and 440 Ma, and plutonism of primarily I-type followed at 375–345 Ma. The Lachlan Group (Stawell and Bendigo zones) of Australia (e.g. VandenBerg et al., 2000; Gray and Foster, 2004; Glen, 2005), Greenland Group of New Zealand (Muir et al., 1996; Adams, 2004), and Swanson Formation of Marie Byrd Land (MBL) (Adams, 1986; Weaver et al., 1991; Pankhurst et al., 1998; Bradshaw, 2007) were all affected.

In the Ford Ranges of MBL (Fig. 2a), calc-alkaline I-type Ford Granodiorite, equated with a convergent margin arc (Weaver et al., 1991), was emplaced at *circa* 375 to 353 Ma (Pankhurst et al., 1998). The Ford plutonic suite intruded Swanson Formation turbidites (Fig. 2a) that had been deformed into NW-plunging folds (Fig. 1) during contraction between 448 and 444 Ma in the Late Ordovician, according to mica cleavage ages (Adams, 2004). A migmatite–granite complex within the Fosdick Mountains gneiss dome (Fig. 2a, b) provides access to exposures of the high-grade equivalents of Swanson Formation and Ford Granodiorite (Siddoway et al., 2004), which attained temperatures in excess of 800 °C according to estimates from mineral equilibria modeling using isochemical phase diagrams (Korhonen et al., 2007, 2008). The temperatures were sufficient to cause voluminous melting and generation of anatexitic granites that are a hybrid mixture of the two sources (Saito et al., 2007a,b). The presence of prismatic igneous zircon and of oscillatory zoned rims upon inherited zircon grains shows that temperatures were sufficiently high to result in the growth of new zircon

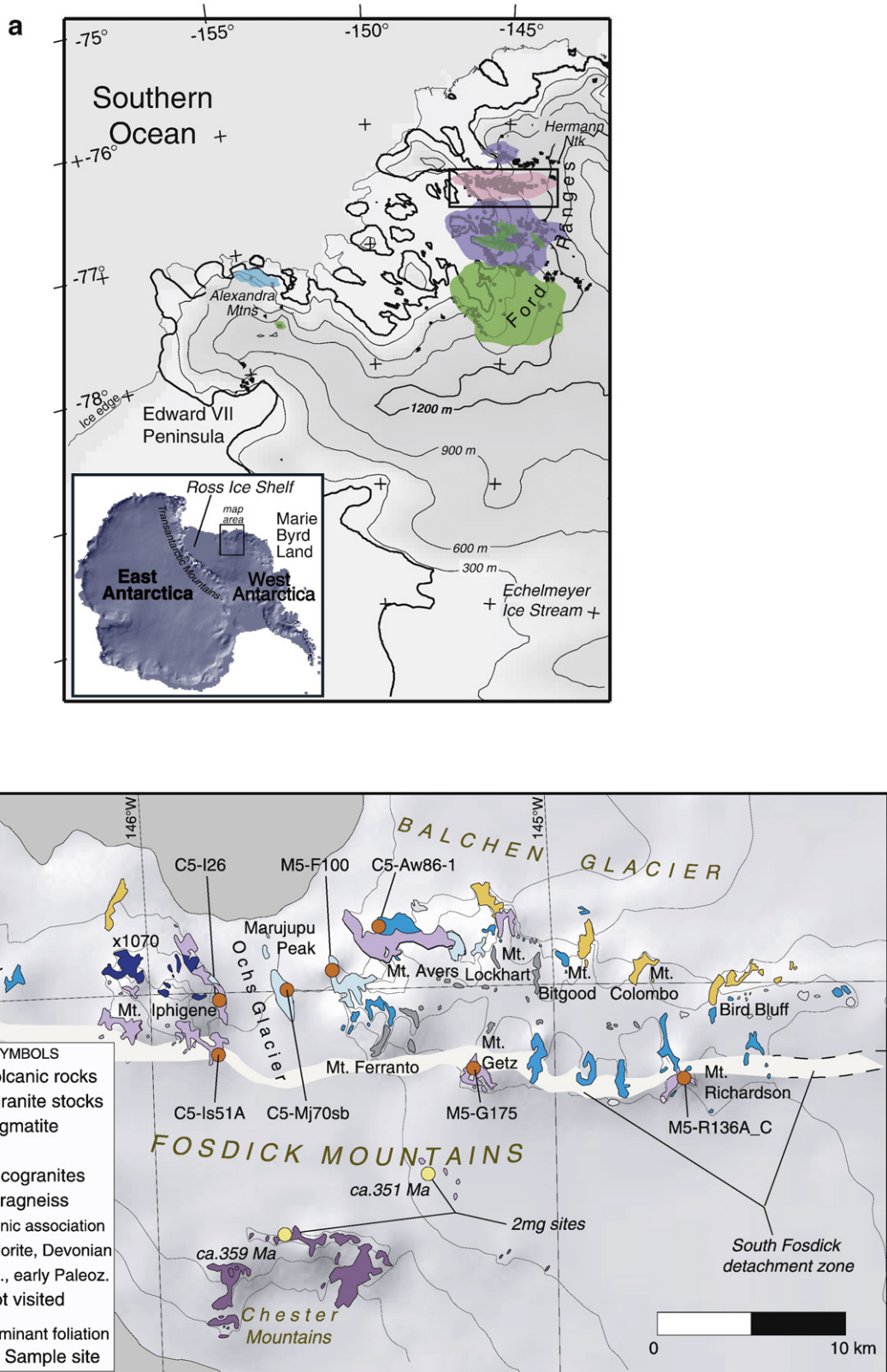


Fig. 2. a. Location of Fosdick Mountains and distribution of Paleozoic rock units within the Ford Ranges of western Marie Byrd Land. Lithological units are: Swanson Formation, green; Ford Granodiorite, purple; Fosdick Mountains migmatite, pink; and Alexandra Mountains migmatite, teal. The inset shows the location of the figure within Antarctica. The box indicates the location of panel b. b. Generalized geological map of the Fosdick Mountains showing lithological units and geographic place names used in the text. Location and age of two-mica granites (label: 2mg) studied by Tulloch et al. (2009) are also indicated.

(>750 °C: Harrison et al., 2007), both as new igneous grains in leucosome/leucogranite and as zoned overgrowths upon preexisting grains. Microstructures indicative of the presence of melt are pervasive (Siddoway et al., 2008).

Because the Fosdick Mountains experienced multiple episodes of HT metamorphism and anatexis (Siddoway et al., 2006; Korhonen et al., 2007, 2008), detailed geochronology is required to delineate the principle plutonic and metamorphic events, and to distinguish the details of the Paleozoic history from subsequent events. We used SHRIMP U–Pb geochronology upon granodiorite, migmatitic monzonogranite gneiss, and discordant leucogranite to determine the timing of Paleozoic plutonism and crustal melting events. Results from 8 samples are presented here, together with structural observations bearing on the strain state during HT metamorphism and anatexis.

2.1. Lithological relationships and structures

Detailed mapping, structural analysis (Siddoway et al., 2004) and metamorphic petrology with *in situ* monazite geochronology (Korhonen et al., 2007, 2008) indicate that rock associations and relict structures formed during Paleozoic orogeny are preserved at deepest structural levels in the central Fosdick Mountains; a hypothesis that is supported by the new geochronology reported in this paper. The central Fosdick range is a migmatite–granite complex with two constituent parts: a layered plutonic association and a residual paragneiss domain. It is thought that HT metamorphism during Paleozoic orogeny depleted the source rocks of melt (Korhonen et al., 2007; Saito et al., 2007a,b), creating a competent, refractory domain that was largely unaffected by Cretaceous tectonism (Siddoway et al., 2008). At higher structural levels in the Fosdick Mountains, Paleozoic intrusives form discrete plutons exceeding 2 km in dimension that are

overprinted by deformation associated with the Cretaceous detachment structure responsible for the exhumation of the Fosdick Mountains gneiss dome (Fig. 2) (McFadden et al., 2007). The Paleozoic plutons are intruded by Cretaceous-aged granites that localized in and beneath the detachment zone (Fig. 2) (McFadden et al., 2008).

Exposures of the central Fosdick range consist of prevalent granite, granodiorite and diorite (Fig. 3), with subordinate metasedimentary gneisses in semi-concordant, laterally continuous layers, meters to decimeters thick, that are visible in semi-vertical rock faces that are 300 to 650 m in height (Fig. 3). The paragneisses are the high-grade equivalents of Swanson Formation of the broader Ford Ranges (Siddoway et al., 2004) and so represent the host rock for the plutonic association. The metaplutonic and metasedimentary gneisses are all migmatitic (e.g. Fig. 4a), exhibiting distinct metamorphic layering and within-source leucosome (e.g. Sawyer, 2008) at mm- to cm-scale. The dominant orientation of compositional boundaries, granite sills, and metamorphic foliation within the plutonic association is subhorizontal (Fig. 4b).

Mineral lineations and hinge lines of small scale folds in migmatitic gneisses of the central Fosdick Mountains are oriented 18, N16E–S16W (Siddoway et al., 2004). Anisotropy of magnetic susceptibility data for this area have a mean K_1 , a proxy for the orientation of the maximum finite strain axis (stretching axis), oriented N19E–S19W (Fig. 4c) (Siddoway et al., 2004).

In addition, discordant structures host granites in sills, dikes and irregular-shaped bodies. The granites generally lack visible internal foliation. Their geochemical and isotope characteristics indicate that the granites are a hybrid mixture of melts derived from melting of both plutonic and metasedimentary host sources (Saito et al., 2007a,b), albeit possibly originating from greater depth or outside the Fosdick complex *per se*.



Fig. 3. Photograph of the layered plutonic association at Marujupu Peak, with plutonic phases labeled. Height of exposure is 270 m.

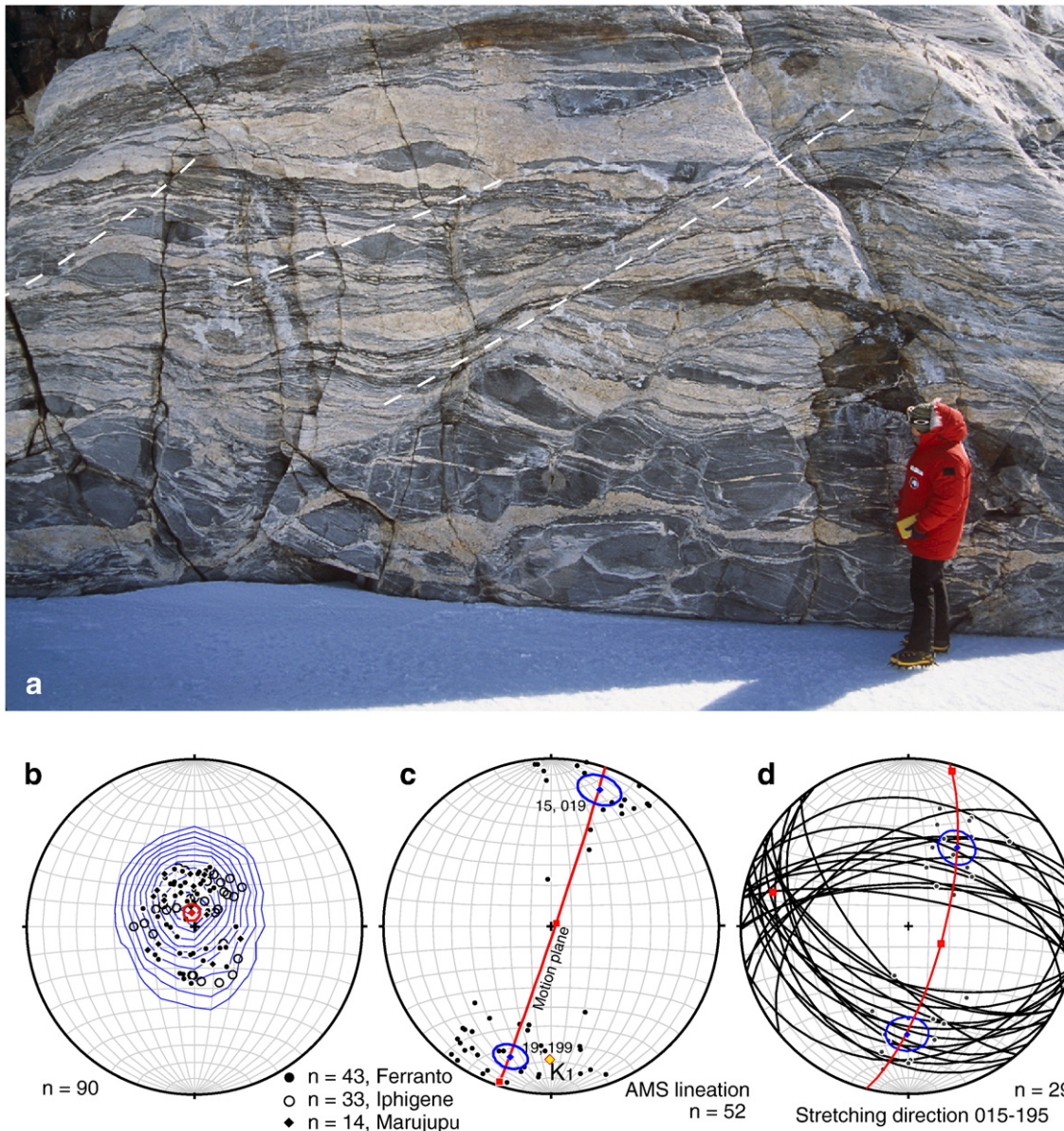


Fig. 4. a. Photograph of granodiorite and diorite hosting semi-concordant sills of granite; all cut by normal-sense shear bands. Location: Marujupu Peak. The shear bands (accentuated with white dashed lines) host granite that is texturally and petrologically continuous with granite in the semi-concordant sills. b. Contoured poles to foliation and compositional layering in the layered plutonic association bordering Ochs Glacier in the central Fosdick Mountains, $n = 90$. c. Mineral lineation measured in the layered plutonic association bordering Ochs Glacier, $n = 52$. The mean K_1 axis oriented 22/181, determined from anisotropy of magnetic susceptibility measurements (Siddoway et al., 2004), is denoted with the diamond symbol. d. Stereographic diagram of planes and poles to planes of conjugate shear bands, Marujupu Peak. The mean poles to planes (blue) were used to determine the extension direction of N15E. The data set includes the structures shown in panel a together with measurements from neighboring outcrops.

In the lower part of the layered plutonic association at Marujupu Peak, extensional structures that host granite overprint compositional boundaries and migmatitic layering. An example is a conjugate shear band array that cuts migmatitic layering but contains granite that lacks internal foliation (Fig. 4a). Geometrical and kinematic analysis of the vein array determines a NNE–SSW stretching direction associated with the normal-sense shear bands (Fig. 4d). The granite emplaced in the shear bands (sample C5-Mj70SB; see below) can thus provide a minimum age for the migmatization.

Throughout this level of the migmatite complex, there are additional examples of systematic, moderately dipping, discordant veins and cm-scale 'knots' of leucogranite, including some that contain euhedral to subhedral cordierite (sample C5-J26, below), that cut foliation and compositional layering. The presence of granite in dilatational structures such as shear bands and veins that postdate the plutonic layering and cut

across the majority of the migmatitic layering suggests that the structures may have acted as conduits for migration of melt (e.g. Bons et al., 2008). In thin section, microstructures indicative of former melt presence include tiny 'beads' of quartz along boundaries of euhedral K-feldspar phenocrysts (Fig. 5a, b) and interconnected networks of optically uniform quartz within sieve-textured K-feldspar (Fig. 5c). The intercrystalline quartz is a probable remnant of an intergranular melt film (Holness and Sawyer, 2008). In outcrops, granite in diffuse masses with indistinct contacts (Fig. 5d) or in discordant dikes (Fig. 5e) cuts across migmatitic foliation developed in units forming the layered plutonic association.

The granites are optimal samples for U–Pb zircon geochronology because their microstructural, geochemical and isotopic characteristics show they are products of HT metamorphism and crustal melting (Saito et al., 2007b; Korhonen et al., 2007). Due to limitations of access in the

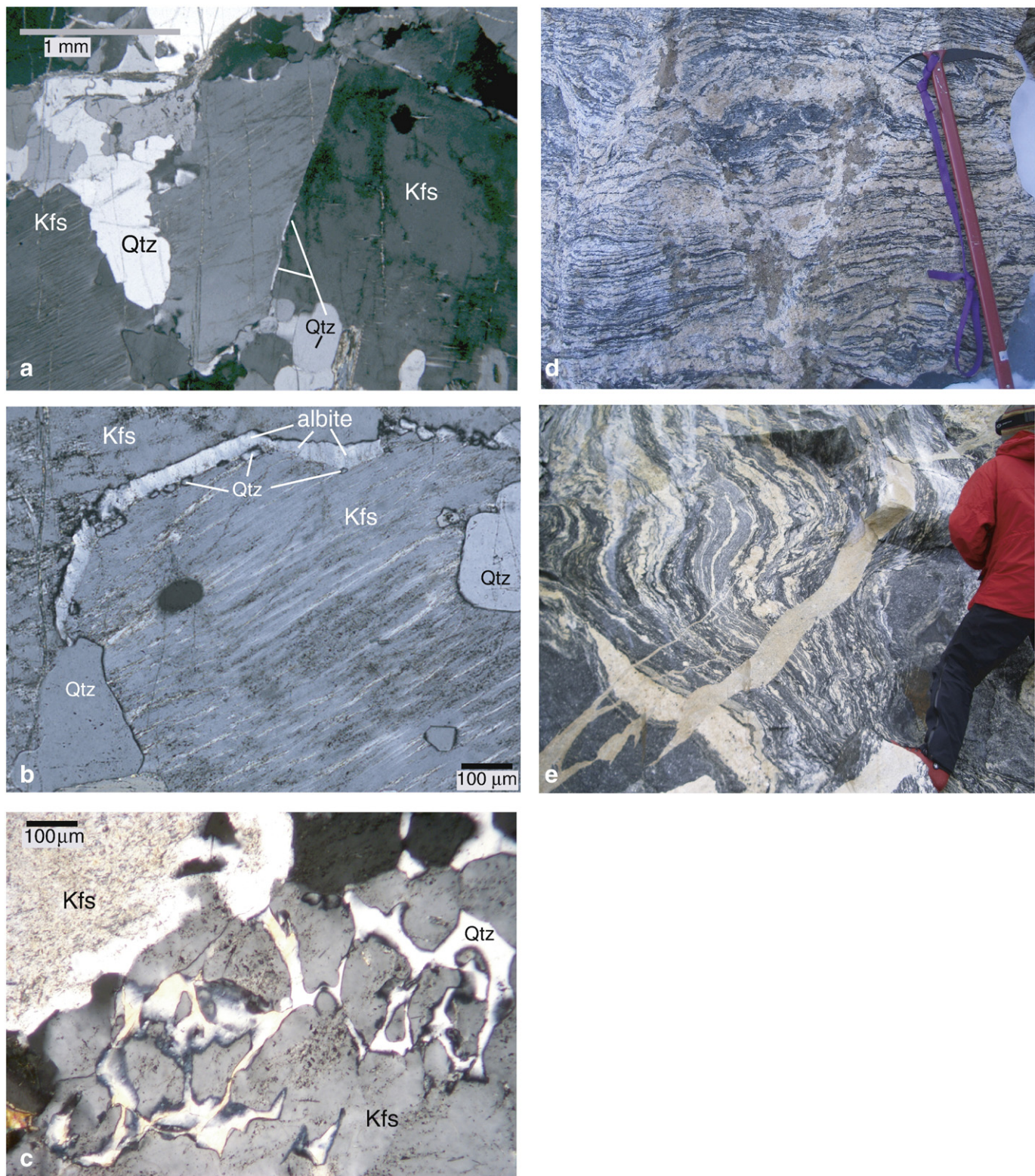


Fig. 5. Microstructural and outcrop evidence for former melt presence within granites emplaced in structural sites. a. Euhedral K-feldspar phenocrysts with intercrystalline quartz along grain boundary as a probable remnant of an intergranular melt film (Holness and Sawyer, 2008), sample C5-Mj70 from Marujupu Peak. b. Subhedral K-feldspar with albite along a grain boundary, in turn ornamented by blebs of quartz, sample C5-Mj70. c. Sieve-textured K-feldspar, with optically uniform quartz filling the interconnected 'pores,' sample C5-Is51A from Mt. Iphigene. d. Outcrop of well-foliated migmatitic gneisses of the layered plutonic association of Mt. Iphigene, cut by discordant cordierite-K-feldspar granite (sample C5-I26) with indistinct contacts that is inferred to be a product of crustal melting during HT metamorphism. The granite sample was collected from this outcrop. Ice axe is 75 cm long. e. Crosscutting granite dike (sample M5-F100) that cuts well-foliated migmatitic gneisses of the layered plutonic association, Mt. Ferranto. Mineral abbreviations in the figure are from Kretz (1983).

glaciated Antarctic setting, however, we could not acquire geometrical data to do kinematic analysis on all of the granite-hosting structures, so as to determine whether they formed in response to far field stresses,

and thus have tectonic significance, or whether they reflect local asperities arising within competent layers during melt movement (e.g. Bons et al., 2008).

3. U-Pb geochronology

3.1. U-Pb zircon geochronology, previously published

Pankhurst et al. (1998) determined a SHRIMP U-Pb zircon age of Ford Granodiorite from sites in the Ford Ranges, the Fosdick Mountains excluded, as 375 ± 5 Ma. They calculated Rb-Sr isochrons for aplites and pegmatites that intrude Ford Granodiorite at two sites, with a result of 330 ± 20 Ma for Hermann Nunatak and 338 ± 3 Ma for the Chester Mountains (for locations: see Fig. 2). Tulloch et al. (2009) determined U-Pb monazite ages of *circa* 359 Ma and *circa* 351 Ma for two-mica granites that intrude Ford Granodiorite at two sites adjacent to the Fosdick Mountains (for locations, see Fig. 2b).

Within the Fosdick range, previously published data for a population of primary magmatic zircon from a garnet-bearing granodiorite orthogneiss at Mt. Bitgood provides an age of 376 ± 7.6 Ma ($n = 12$; MSWD 7.3) (Siddoway et al., 2004). Based on new mapping of 2005–2006, the unit is a member of the Ford Granodiorite suite. Single zircon analyses (Saito et al., 2007a,b) using laser ablation inductively coupled plasma mass spectrometry (LA-ICP-MS) methods were acquired as part of an investigation of granite petrogenesis in the Fosdick Mountains. Prismatic euhedral zircons from four granites yield Carboniferous ages of 358 to 336 Ma (combined ages from analyses of 5 to 8 grains). Zircon overgrowths of Permian age were noted in the study. One granite contained igneous zircon of latest Devonian age, determined from 5 analyses as 357.6 ± 8.3 Ma (MSWD 1.1) (Saito et al., 2007b). Minimal information is available on zircon formed during metamorphism, however there are preliminary data from *in situ* monazite geochronology of paragneisses, acquired by electron probe microanalysis (Korhonen et al., 2007). Ages of *circa* 365–340 Ma are determined for monazite inclusions within garnet that is part of the peak pressure–temperature (*P-T*) assemblage. Peak conditions reached an estimated 820–870 °C and 7–12 kbar based on isochemical phase diagrams (pseudosections; Korhonen et al., 2008).

3.2. SHRIMP U-Pb zircon geochronology and REE analysis

3.2.1. Analytical techniques

Zircon mineral separates were prepared from bulk rock samples by crushing, gravity and magnetic separation, heavy liquids, and hand picking under fiber optic illumination at the Australian National University Research School of Earth Sciences (ANU-RSES). Zircons were mounted in epoxy, ground to approximately half-thickness, and polished with 3 µm and 1 µm diamond suspension. Cathodoluminescence (CL) images for zircon characterization (Fig. 6) were collected using scanning electron microscope, together with transmitted and reflected light images using a petrographic microscope. Zircon U-Th-Pb isotopic analyses were collected using SHRIMP II and SHRIMP RG at ANU-RSES, following procedures described in Williams (1998). Data were reduced using the SQUID Excel Macro of Ludwig (2001). The $^{206}\text{U}/^{238}\text{Pb}$ ratios have been normalized relative to a value of 0.0668 for the Temora reference zircon, equivalent to an age of 417 Ma (Black et al., 2003).

Data for eight samples appear in Table 1; uncertainties given for individual analyses (ratios and ages) are at the one-sigma level. Probability density plots with stacked histograms and weighted mean $^{206}\text{U}/^{238}\text{Pb}$ ages for coherent groupings (Figs. 7, 8) and Tera and Wasserburg (1972) concordia plots (Figs. 7, 8) were calculated using ISOPLOT/EX (Ludwig, 2003). ISOPLOT/EX employs the "Mixture Modeling" algorithm of Sambridge and Compston (1994) to unmix statistical age populations or groupings, which are in turn used to calculate weighted mean $^{206}\text{Pb}/^{238}\text{U}$ ages. Uncertainties in the calculated ages are reported as 95% confidence limits.

We analysed rare earth element (REE) and trace element concentrations for zircons of known age in order to acquire geochemical information bearing on zircon formation processes and source material (e.g. Ireland and Wlotzka, 1992; Maas et al., 1992). REE data were acquired using SHRIMP RG at ANU-RSES for selected spots that had been analysed

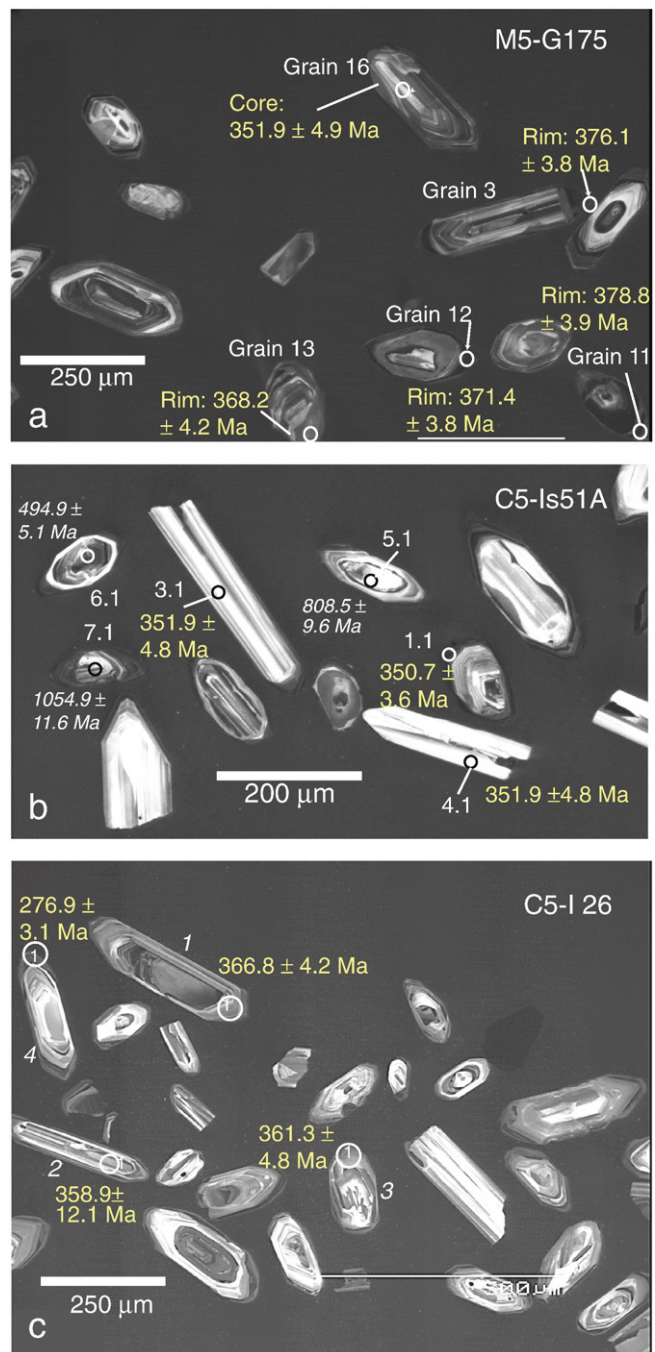


Fig. 6. Cathodoluminescence images, analysis spots, and ages for three samples. a. Sample C5-Is51A, porphyritic monzogranite orthogneiss of southeastern Mt. Iphigene. b. Sample M5-G175, biotite granodiorite of Mt. Getz. c. Sample C5-I26, cordierite-K-feldspar granite (Fig. 5d), central eastern Mt. Iphigene.

for U-Pb–Th geochronology. The energy filtering method was used to reduce interferences (Ireland and Wlotzka, 1992; Guo et al., 1996) and in most instances two isotopes were measured (Table 2) so that the isotopic ratios could be used to check for isobaric interferences. Operating conditions and data reduction methods are similar to those described in Hoskin (1998). REE detection limits are in the vicinity of 0.01 ppm for the analysis spots that are 30 µm across and a few micrometers deep.

3.2.2. Study samples

Samples of regionally widespread granitoids that were selected for U-Pb zircon geochronology include dark, medium-grained, equigranular biotite granodiorite that forms large plutons at Mt. Getz and Mt.

Table 1

Summary of SHRIMP U–Pb–Th zircon results for 8 samples.

| Grain spot | U (ppm) | Th (ppm) | Th/U | $^{206}\text{Pb}^*$ (ppm) | $^{204}\text{Pb}/^{206}\text{Pb}$ | $f_{206} \%$ | Total | | | Radiogenic | | Age (Ma) | | | |
|--|------------|-------------|------|------------------------------|-----------------------------------|--------------|----------------------------------|--------|-----------------------------------|------------|----------------------------------|----------|----------------------------------|--------|------|
| | | | | | | | $^{238}\text{U}/^{206}\text{Pb}$ | ± | $^{207}\text{Pb}/^{206}\text{Pb}$ | ± | $^{206}\text{Pb}/^{238}\text{U}$ | ± | $^{206}\text{Pb}/^{238}\text{U}$ | ± | |
| <i>M5-G175</i> | | | | | | | | | | | | | | | |
| 1.1 | c | 801 | 2 | 0.002 | 36.0 | 0.000266 | 0.24 | 19.113 | 0.209 | 0.0549 | 0.0006 | 0.0522 | 0.0006 | 328.0 | 3.5 |
| 1.2 | r | 724 | 565 | 0.781 | 35.2 | 0.000291 | 0.44 | 17.673 | 0.191 | 0.0571 | 0.0006 | 0.0563 | 0.0006 | 353.3 | 3.8 |
| 2.1 | r | 866 | 3 | 0.003 | 42.7 | 0.000045 | 0.41 | 17.412 | 0.186 | 0.0570 | 0.0005 | 0.0572 | 0.0006 | 358.6 | 3.8 |
| 2.2 | c | 88 | 30 | 0.334 | 7.9 | 0.000727 | 1.38 | 9.610 | 0.136 | 0.0720 | 0.0013 | 0.1026 | 0.0015 | 629.8 | 8.7 |
| 3.1 | r | 1767 | 7 | 0.004 | 91.6 | 0.000229 | 0.50 | 16.562 | 0.172 | 0.0581 | 0.0003 | 0.0601 | 0.0006 | 376.1 | 3.8 |
| 4.1 | r | 566 | 3 | 0.005 | 28.7 | 0.000519 | 0.48 | 16.974 | 0.187 | 0.0577 | 0.0006 | 0.0586 | 0.0007 | 367.3 | 4.0 |
| 5.1 | r | 733 | 7 | 0.009 | 37.0 | 0.000196 | 0.19 | 17.006 | 0.185 | 0.0555 | 0.0005 | 0.0587 | 0.0006 | 367.6 | 3.9 |
| 6.1 | r | 953 | 6 | 0.007 | 47.5 | 0.000118 | 0.18 | 17.223 | 0.185 | 0.0553 | 0.0005 | 0.0580 | 0.0006 | 363.2 | 3.8 |
| 7.1 | r | 364 | 77 | 0.211 | 18.6 | 0.001068 | 2.46 | 16.867 | 0.198 | 0.0736 | 0.0010 | 0.0578 | 0.0007 | 362.4 | 4.2 |
| 8.1 | r | 1783 | 7 | 0.004 | 91.4 | 0.000134 | 0.24 | 16.759 | 0.175 | 0.0560 | 0.0004 | 0.0595 | 0.0006 | 372.7 | 3.8 |
| 9.1 | r | 470 | 58 | 0.123 | 23.5 | 0.001112 | 1.42 | 17.162 | 0.193 | 0.0652 | 0.0020 | 0.0574 | 0.0007 | 360.1 | 4.1 |
| 10.1 | r | 796 | 12 | 0.015 | 40.7 | 0.000136 | 0.33 | 16.803 | 0.181 | 0.0567 | 0.0005 | 0.0593 | 0.0006 | 371.5 | 3.9 |
| 11.1 | r | 1613 | 11 | 0.007 | 83.9 | 0.000136 | 0.11 | 16.505 | 0.174 | 0.0551 | 0.0004 | 0.0605 | 0.0006 | 378.8 | 3.9 |
| 12.1 | r | 2236 | 24 | 0.011 | 114.1 | 0.000099 | 0.17 | 16.833 | 0.174 | 0.0554 | 0.0003 | 0.0593 | 0.0006 | 371.4 | 3.8 |
| 13.1 | r | 1158 | 11 | 0.010 | 58.9 | 0.000299 | 0.69 | 16.895 | 0.194 | 0.0595 | 0.0005 | 0.0588 | 0.0007 | 368.2 | 4.2 |
| 14.1 | r | 2219 | 26 | 0.012 | 116.8 | 0.000070 | 0.02 | 16.316 | 0.169 | 0.0544 | 0.0003 | 0.0613 | 0.0006 | 383.4 | 3.9 |
| 15.1 | c | 275 | 147 | 0.532 | 14.1 | 0.000423 | 1.18 | 16.728 | 0.203 | 0.0635 | 0.0012 | 0.0591 | 0.0007 | 370.0 | 4.4 |
| 16.1 | c | 141 | 55 | 0.394 | 7.1 | 0.002117 | 4.03 | 17.106 | 0.236 | 0.0860 | 0.0022 | 0.0561 | 0.0008 | 351.9 | 4.9 |
| Note: Error in Temora reference zircon calibration was 0.39% for the analytical session. | | | | | | | | | | | | | | | |
| <i>M5-R136A (selected analysis spots of Paleozoic age)</i> | | | | | | | | | | | | | | | |
| 2.2_A | c | 384 | 95 | 0.247 | 17.3 | 0.000234 | 0.30 | 19.100 | 0.222 | 0.0554 | 0.0006 | 0.0522 | 0.0006 | 328.0 | 3.8 |
| 4.1_A | c | 446 | 137 | 0.307 | 22.7 | 0.000276 | 0.62 | 16.879 | 0.183 | 0.0590 | 0.0006 | 0.0589 | 0.0006 | 368.8 | 3.9 |
| 4.2_A | c | 122 | 1 | 0.010 | 9.9 | 0.000752 | 1.54 | 10.631 | 0.141 | 0.0717 | 0.0011 | 0.0926 | 0.0013 | 571.0 | 7.4 |
| 5.1_A | r | 1500 | 50 | 0.033 | 75.4 | 0.000047 | 0.19 | 17.105 | 0.193 | 0.0554 | 0.0004 | 0.0584 | 0.0007 | 365.6 | 4.1 |
| 8.1_A | r | 470 | 43 | 0.092 | 17.3 | 0.000179 | 0.66 | 23.304 | 0.267 | 0.0569 | 0.0008 | 0.0426 | 0.0005 | 269.1 | 3.1 |
| 14.1_A | c | 271 | 97 | 0.360 | 13.4 | 0.000395 | 1.12 | 17.355 | 0.210 | 0.0627 | 0.0010 | 0.0570 | 0.0007 | 357.2 | 4.3 |
| 24.1_A | c | 393 | 43 | 0.110 | 12.9 | 0.000700 | 0.80 | 26.105 | 0.322 | 0.0574 | 0.0015 | 0.0380 | 0.0005 | 240.4 | 3.0 |
| 25.1_A | c | 198 | 180 | 0.910 | 9.9 | 0.000434 | 0.92 | 17.166 | 0.232 | 0.0612 | 0.0013 | 0.0577 | 0.0008 | 361.7 | 4.8 |
| 26.1_A | c | 990 | 731 | 0.739 | 50.0 | 0.000056 | 0.09 | 17.016 | 0.185 | 0.0546 | 0.0007 | 0.0587 | 0.0006 | 367.8 | 3.9 |
| <i>M5-R136C (selected analysis spots of Paleozoic age)</i> | | | | | | | | | | | | | | | |
| 1.1_C | r | 889 | 45 | 0.051 | 44.4 | 0.000007 | 0.17 | 17.187 | 0.201 | 0.0552 | 0.0005 | 0.0581 | 0.0007 | 364.0 | 4.2 |
| 1.2_C | c | 785 | 230 | 0.293 | 36.0 | 0.000046 | 0.21 | 18.713 | 0.202 | 0.0549 | 0.0005 | 0.0533 | 0.0006 | 334.9 | 3.6 |
| 12.1_C | r | 1524 | 492 | 0.323 | 61.1 | — | 0.12 | 21.427 | 0.225 | 0.0532 | 0.0004 | 0.0466 | 0.0005 | 293.7 | 3.0 |
| 14.1_C | c | 450 | 144 | 0.321 | 22.1 | 0.000259 | 0.03 | 17.498 | 0.205 | 0.0539 | 0.0008 | 0.0571 | 0.0007 | 358.2 | 4.1 |
| 19.1_C | c | 1059 | 652 | 0.615 | 53.3 | 0.000069 | 0.08 | 17.059 | 0.184 | 0.0546 | 0.0005 | 0.0586 | 0.0006 | 366.9 | 3.9 |
| 2.1_C | c | 1305 | 34 | 0.026 | 67.4 | — | <0.01 | 16.624 | 0.274 | 0.0530 | 0.0004 | 0.0602 | 0.0010 | 377.1 | 6.1 |
| 6.2_C | c | 953 | 587 | 0.616 | 48.4 | 0.000031 | 0.03 | 16.901 | 0.184 | 0.0543 | 0.0005 | 0.0591 | 0.0007 | 370.5 | 4.0 |
| 8.1_C | c | 188 | 75 | 0.402 | 9.4 | — | 0.47 | 17.150 | 0.228 | 0.0576 | 0.0012 | 0.0580 | 0.0008 | 363.7 | 4.8 |
| 8.2_C | r | 2066 | 53 | 0.026 | 107.4 | — | <0.01 | 16.535 | 0.172 | 0.0541 | 0.0003 | 0.0605 | 0.0006 | 378.6 | 3.9 |
| Note: Error in Temora reference zircon calibration was 0.39% for the analytical session. | | | | | | | | | | | | | | | |
| <i>C5-Is51A</i> | | | | | | | | | | | | | | | |
| 1.1 | r | 2337 | 29 | 0.012 | 112.3 | — | 0.05 | 17.878 | 0.185 | 0.0539 | 0.0003 | 0.0559 | 0.0006 | 350.7 | 3.6 |
| 2.1 | r | 1669 | 14 | 0.009 | 81.9 | — | <0.01 | 17.503 | 0.184 | 0.0536 | 0.0005 | 0.0571 | 0.0006 | 358.2 | 3.7 |
| 3.1 | c | 83 | 56 | 0.672 | 4.0 | — | 0.23 | 17.749 | 0.294 | 0.0554 | 0.0022 | 0.0562 | 0.0010 | 352.6 | 5.8 |
| 4.1 | c | 167 | 87 | 0.519 | 8.0 | — | 0.08 | 17.807 | 0.245 | 0.0542 | 0.0013 | 0.0561 | 0.0008 | 351.9 | 4.8 |
| 5.1 | c | 218 | 33 | 0.152 | 25.2 | — | 0.86 | 7.420 | 0.091 | 0.0731 | 0.0009 | 0.1336 | 0.0017 | 808.5 | 9.6 |
| 6.1 | c | 1113 | 599 | 0.539 | 76.3 | — | <0.01 | 12.537 | 0.133 | 0.0568 | 0.0004 | 0.0798 | 0.0009 | 494.9 | 5.1 |
| 7.1 | c | 335 | 199 | 0.595 | 51.3 | — | 0.13 | 5.617 | 0.064 | 0.0756 | 0.0006 | 0.1778 | 0.0021 | 1054.9 | 11.6 |
| 8.1 | c | 748 | 30 | 0.040 | 35.7 | — | 0.09 | 18.020 | 0.203 | 0.0542 | 0.0006 | 0.0554 | 0.0006 | 347.9 | 3.9 |
| 9.1 | c | 1182 | 634 | 0.536 | 86.5 | — | <0.01 | 11.750 | 0.124 | 0.0576 | 0.0004 | 0.0851 | 0.0009 | 526.7 | 5.5 |
| 10.1 | c | 339 | 213 | 0.629 | 16.3 | — | 0.02 | 17.839 | 0.223 | 0.0537 | 0.0009 | 0.0560 | 0.0007 | 351.6 | 4.3 |
| 11.1 | c | 79 | 34 | 0.432 | 7.7 | 0.000047 | 0.18 | 8.806 | 0.136 | 0.0640 | 0.0015 | 0.1134 | 0.0018 | 692.2 | 10.5 |
| 12.1 | c | 385 | 81 | 0.211 | 18.7 | 0.000135 | <0.01 | 17.687 | 0.217 | 0.0531 | 0.0008 | 0.0566 | 0.0007 | 354.8 | 4.3 |
| 13.1 | c | 340 | 227 | 0.666 | 17.5 | 0.000259 | 0.12 | 16.729 | 0.204 | 0.0551 | 0.0009 | 0.0597 | 0.0007 | 373.8 | 4.5 |
| 14.1 | c | 268 | 182 | 0.677 | 13.3 | — | 0.18 | 17.376 | 0.220 | 0.0552 | 0.0011 | 0.0574 | 0.0007 | 360.1 | 4.5 |
| Note: Error in Temora reference zircon calibration was 0.39% for the analytical session. | | | | | | | | | | | | | | | |
| <i>M5-F100</i> | | | | | | | | | | | | | | | |
| 1.1 | r | 1957 | 60 | 0.031 | 31.3 | 0.000479 | 0.84 | 53.644 | 0.575 | 0.0551 | 0.0007 | 0.0185 | 0.0002 | 118.1 | 1.3 |
| 1.2 | c | 287 | 182 | 0.636 | 14.5 | 0.000615 | 1.63 | 16.932 | 0.204 | 0.0670 | 0.0013 | 0.0581 | 0.0007 | 364.0 | 4.4 |
| 2.1 | r | 1877 | 5 | 0.002 | 79.0 | 0.000502 | 0.99 | 20.425 | 0.212 | 0.0604 | 0.0004 | 0.0485 | 0.0005 | 305.2 | 3.1 |
| 3.1 | r | 1291 | 30 | 0.023 | 66.9 | 0.000304 | 0.58 | 16.579 | 0.191 | 0.0588 | 0.0005 | 0.0600 | 0.0007 | 375.4 | 4.2 |
| 4.1 | c | 118 | 46 | 0.392 | 5.1 | 0.001564 | 2.55 | 19.995 | 0.523 | 0.0730 | 0.0020 | 0.0487 | 0.0013 | 306.8 | 7.9 |
| 5.1 | c | 614 | 169 | 0.275 | 31.6 | 0.000339 | 0.22 | 16.699 | 0.188 | 0.0558 | 0.0007 | 0.0598 | 0.0007 | 374.1 | 4.1 |
| 6.1 | c | 1337 | 105 | 0.078 | 64.9 | 0.001158 | 1.60 | 17.699 | 0.210 | 0.0663 | 0.0007 | 0.0556 | 0.0007 | 348.8 | 4.1 |
| 7.1 | c | 612 | 27 | 0.044 | 37.7 | 0.000154 | 0.54 | 1 | | | | | | | |

Table 1 (continued)

| Grain spot | U (ppm) | Th (ppm) | Th/U | $^{206}\text{Pb}^*$ (ppm) | $^{204}\text{Pb}/^{206}\text{Pb}$ | f ₂₀₆ % | Total | | | | Radiogenic | | Age (Ma) | | |
|--|---------|----------|------|---------------------------|-----------------------------------|--------------------|----------------------------------|--------|-----------------------------------|--------|----------------------------------|--------|----------------------------------|-------|------|
| | | | | | | | $^{238}\text{U}/^{206}\text{Pb}$ | ± | $^{207}\text{Pb}/^{206}\text{Pb}$ | ± | $^{206}\text{Pb}/^{238}\text{U}$ | ± | $^{206}\text{Pb}/^{238}\text{U}$ | ± | |
| M5-F100 | | | | | | | | | | | | | | | |
| 11.1 | c | 1403 | 105 | 0.075 | 160.6 | 0.000118 | 0.77 | 7.501 | 0.079 | 0.0722 | 0.0004 | 0.1323 | 0.0014 | 800.9 | 8.1 |
| 12.1 | c | 384 | 524 | 1.364 | 28.0 | 0.000675 | 1.29 | 11.785 | 0.137 | 0.0682 | 0.0010 | 0.0838 | 0.0010 | 518.5 | 5.9 |
| 13.1 | c | 199 | 47 | 0.239 | 10.1 | 0.001052 | 1.65 | 16.855 | 0.226 | 0.0672 | 0.0014 | 0.0584 | 0.0008 | 365.6 | 4.9 |
| Note: Error in Temora reference zircon calibration was 0.39% for the analytical session. | | | | | | | | | | | | | | | |
| C5-I26 | | | | | | | | | | | | | | | |
| 1.1 | r | 414 | 62 | 0.15 | 20.8 | – | <0.01 | 17.080 | 0.201 | 0.0539 | 0.0005 | 0.0585 | 0.0007 | 366.8 | 4.2 |
| 2.1 | c | 304 | 74 | 0.24 | 15.0 | 0.000078 | 0.29 | 17.416 | 0.597 | 0.0561 | 0.0007 | 0.0573 | 0.0020 | 358.9 | 12.1 |
| 3.1 | r | 350 | 40 | 0.12 | 17.3 | 0.000072 | 0.14 | 17.320 | 0.232 | 0.0549 | 0.0005 | 0.0577 | 0.0008 | 361.3 | 4.8 |
| 4.1 | r | 1187 | 10 | 0.01 | 44.8 | 0.000044 | 0.20 | 22.742 | 0.254 | 0.0534 | 0.0003 | 0.0439 | 0.0005 | 276.9 | 3.1 |
| 5.1 | r | 1687 | 8 | 0.00 | 84.7 | 0.000017 | 0.05 | 17.114 | 0.177 | 0.0543 | 0.0002 | 0.0584 | 0.0006 | 365.9 | 3.7 |
| 5.2 | r | 740 | 13 | 0.02 | 36.9 | 0.000036 | 0.04 | 17.238 | 0.190 | 0.0542 | 0.0005 | 0.0580 | 0.0006 | 363.4 | 3.9 |
| 5.3 | c | 211 | 157 | 0.74 | 10.4 | 0.000315 | 0.10 | 17.391 | 0.214 | 0.0546 | 0.0008 | 0.0574 | 0.0007 | 360.1 | 4.4 |
| 6.1 | c | 113 | 35 | 0.31 | 5.3 | 0.000644 | 0.30 | 18.443 | 0.244 | 0.0557 | 0.0012 | 0.0541 | 0.0007 | 339.4 | 4.4 |
| 7.1 | c | 157 | 63 | 0.40 | 8.0 | 0.000217 | 0.15 | 16.767 | 0.558 | 0.0552 | 0.0010 | 0.0596 | 0.0020 | 372.9 | 12.2 |
| 8.1 | r | 307 | 47 | 0.15 | 15.5 | 0.000002 | 0.10 | 16.987 | 0.194 | 0.0547 | 0.0007 | 0.0588 | 0.0007 | 368.4 | 4.1 |
| 9.1 | c | 86 | 46 | 0.54 | 4.3 | 0.000492 | 0.41 | 17.035 | 0.251 | 0.0572 | 0.0013 | 0.0585 | 0.0009 | 366.3 | 5.3 |
| 10.1 | r | 342 | 57 | 0.17 | 17.5 | 0.000069 | 0.05 | 16.809 | 0.190 | 0.0544 | 0.0006 | 0.0595 | 0.0007 | 372.4 | 4.1 |
| 11.1 | c | 254 | 150 | 0.59 | 12.8 | 0.000201 | 0.22 | 17.037 | 0.198 | 0.0557 | 0.0008 | 0.0586 | 0.0007 | 366.9 | 4.2 |
| 12.1 | r | 378 | 72 | 0.19 | 18.9 | 0.000136 | 0.03 | 17.209 | 0.193 | 0.0541 | 0.0006 | 0.0581 | 0.0007 | 364.0 | 4.0 |
| 13.1 | c | 544 | 62 | 0.11 | 27.1 | 0.000103 | 0.00 | 17.237 | 0.195 | 0.0539 | 0.0006 | 0.0580 | 0.0007 | 363.5 | 4.0 |
| 14.1 | r | 1610 | 17 | 0.01 | 78.4 | 0.000046 | 0.00 | 17.642 | 0.186 | 0.0536 | 0.0003 | 0.0567 | 0.0006 | 355.4 | 3.7 |
| Note: Error in Temora reference zircon calibration was 0.29% for the analytical session. | | | | | | | | | | | | | | | |
| C5-Mj70-SB | | | | | | | | | | | | | | | |
| 1.1 | r | 3161 | 19 | 0.006 | 48.6 | – | <0.01 | 55.916 | 0.584 | 0.0481 | 0.0004 | 0.0179 | 0.0002 | 114.3 | 1.2 |
| 1.2 | c | 490 | 50 | 0.102 | 43.4 | – | 0.18 | 9.705 | 0.115 | 0.0623 | 0.0008 | 0.1028 | 0.0012 | 631.1 | 7.3 |
| 2.1 | r | 2691 | 16 | 0.006 | 39.7 | – | 0.08 | 58.288 | 0.612 | 0.0489 | 0.0005 | 0.0171 | 0.0002 | 109.6 | 1.1 |
| 3.1 | r | 2442 | 93 | 0.038 | 51.7 | 0.000006 | 0.16 | 40.578 | 0.429 | 0.0504 | 0.0004 | 0.0246 | 0.0003 | 156.7 | 1.6 |
| 4.1 | r | 1092 | 157 | 0.144 | 59.5 | – | <0.01 | 15.755 | 0.181 | 0.0527 | 0.0029 | 0.0636 | 0.0008 | 397.6 | 4.7 |
| 5.1 | r | 1768 | 34 | 0.019 | 110.9 | – | 0.09 | 13.696 | 0.143 | 0.0568 | 0.0003 | 0.0729 | 0.0008 | 453.9 | 4.7 |
| 6.1 | r | 602 | 92 | 0.152 | 31.8 | – | 0.12 | 16.274 | 0.179 | 0.0553 | 0.0006 | 0.0614 | 0.0007 | 384.0 | 4.1 |
| 7.1 | r | 1800 | 73 | 0.041 | 50.1 | 0.000474 | 1.24 | 30.876 | 0.325 | 0.0601 | 0.0005 | 0.0320 | 0.0003 | 203.0 | 2.1 |
| 8.1 | r | 957 | 23 | 0.024 | 37.2 | – | 0.85 | 22.126 | 0.241 | 0.0587 | 0.0006 | 0.0448 | 0.0005 | 282.6 | 3.0 |
| 9.1 | r | 937 | 22 | 0.023 | 45.4 | 0.000076 | 0.13 | 17.752 | 0.190 | 0.0546 | 0.0005 | 0.0563 | 0.0006 | 352.8 | 3.7 |
| 10.1 | r | 1292 | 23 | 0.018 | 48.2 | 0.000005 | 0.15 | 23.037 | 0.245 | 0.0529 | 0.0005 | 0.0433 | 0.0005 | 273.5 | 2.9 |
| 11.1 | r | 1268 | 38 | 0.030 | 27.9 | – | 0.44 | 39.118 | 0.429 | 0.0528 | 0.0006 | 0.0255 | 0.0003 | 162.0 | 1.8 |
| 12.1 | r | 1420 | 10 | 0.007 | 36.9 | – | 1.73 | 33.036 | 0.353 | 0.0636 | 0.0006 | 0.0297 | 0.0003 | 189.0 | 2.0 |
| 13.1 | r | 2958 | 19 | 0.006 | 42.4 | 0.000023 | 0.04 | 59.883 | 0.631 | 0.0485 | 0.0005 | 0.0167 | 0.0002 | 106.7 | 1.1 |
| 14.1 | r | 1589 | 50 | 0.032 | 62.0 | – | 1.22 | 22.024 | 0.232 | 0.0617 | 0.0004 | 0.0449 | 0.0005 | 282.8 | 2.9 |
| 15.1 | r | 895 | 56 | 0.063 | 43.3 | – | 0.11 | 17.735 | 0.190 | 0.0545 | 0.0005 | 0.0563 | 0.0006 | 353.2 | 3.7 |
| 16.1 | r | 1929 | 128 | 0.066 | 96.5 | – | 0.08 | 17.177 | 0.179 | 0.0545 | 0.0003 | 0.0582 | 0.0006 | 364.5 | 3.7 |
| 17.1 | r | 1372 | 68 | 0.049 | 83.1 | – | 1.37 | 14.186 | 0.149 | 0.0666 | 0.0004 | 0.0695 | 0.0007 | 433.3 | 4.5 |
| 18.1 | r | 5072 | 15 | 0.003 | 80.8 | 0.000049 | 0.03 | 53.936 | 0.557 | 0.0486 | 0.0003 | 0.0185 | 0.0002 | 118.4 | 1.2 |
| 19.1 | r | 1784 | 21 | 0.012 | 41.3 | – | 0.43 | 37.069 | 0.436 | 0.0529 | 0.0006 | 0.0269 | 0.0003 | 170.9 | 2.0 |
| 20.1 | r | 1280 | 91 | 0.071 | 63.3 | – | 0.22 | 17.359 | 0.183 | 0.0555 | 0.0004 | 0.0575 | 0.0006 | 360.3 | 3.7 |
| 21.1 | r | 1173 | 31 | 0.026 | 23.3 | – | 0.36 | 43.213 | 0.474 | 0.0519 | 0.0012 | 0.0231 | 0.0003 | 146.9 | 1.6 |
| 22.1 | r | 1708 | 8 | 0.004 | 28.6 | – | 0.25 | 51.400 | 0.593 | 0.0505 | 0.0006 | 0.0194 | 0.0002 | 123.9 | 1.4 |
| 23.1 | r | 1775 | 8 | 0.005 | 33.8 | 0.000089 | 0.32 | 45.131 | 0.484 | 0.0514 | 0.0007 | 0.0221 | 0.0002 | 140.8 | 1.5 |
| 24.1 | r | 1473 | 9 | 0.006 | 43.5 | – | 0.45 | 29.073 | 0.324 | 0.0541 | 0.0008 | 0.0342 | 0.0004 | 217.0 | 2.4 |
| 25.1 | r | 2655 | 24 | 0.009 | 62.2 | – | 0.27 | 36.705 | 0.384 | 0.0517 | 0.0004 | 0.0272 | 0.0003 | 172.8 | 1.8 |
| Note: Error in Temora reference zircon calibration was 0.39% for the analytical session. | | | | | | | | | | | | | | | |
| C6-AW86-1 | | | | | | | | | | | | | | | |
| 1.1 | c | 249 | 146 | 0.588 | 12.1 | 0.000062 | 0.63 | 17.62 | 0.25 | 0.0587 | 0.0018 | 0.0564 | 0.0008 | 353.7 | 5.0 |
| 1.2 | r | 222 | 85 | 0.382 | 11.2 | – | <0.01 | 16.97 | 0.19 | 0.0536 | 0.0007 | 0.0589 | 0.0007 | 369.2 | 4.2 |
| 2.1 | c | 291 | 165 | 0.566 | 14.5 | 0.000060 | <0.01 | 17.22 | 0.19 | 0.0537 | 0.0006 | 0.0581 | 0.0007 | 363.9 | 4.0 |
| 2.2 | r | 2346 | 98 | 0.042 | 41.1 | – | <0.01 | 49.09 | 0.52 | 0.0486 | 0.0003 | 0.0204 | 0.0002 | 130.0 | 1.4 |
| 3.1 | r | 631 | 19 | 0.031 | 9.3 | 0.000279 | 0.15 | 58.30 | 0.65 | 0.0494 | 0.0009 | 0.0171 | 0.0002 | 109.5 | 1.2 |
| 3.2 | c | 958 | 252 | 0.263 | 47.4 | 0.000030 | 0.02 | 17.36 | 0.18 | 0.0540 | 0.0003 | 0.0576 | 0.0006 | 361.0 | 3.7 |
| 4.1 | r | 793 | 21 | 0.026 | 11.4 | 0.000129 | 0.06 | 59.75 | 0.65 | 0.0487 | 0.0006 | 0.0167 | 0.0002 | 106.9 | 1.2 |
| 4.2 | c | 205 | 83 | 0.403 | 10.0 | 0.000048 | 0.08 | 17.57 | 0.20 | 0.0543 | 0.0007 | 0.0569 | 0.0007 | 356.5 | 4.0 |
| 5.1 | r | 638 | 30 | 0.047 | 9.2 | 0.000172 | 0.74 | 59.76 | 0.66 | 0.0540 | 0.0008 | 0.0166 | 0.0002 | 106.2 | 1.2 |
| 5.2 | c | 220 | 63 | 0.286 | 10.7 | 0.000056 | <0.01 | 17.65 | 0.20 | 0.0536 | 0.0007 | 0.0567 | 0.0007 | 355.4 | 4.0 |
| 6.1 | r | 1609 | 61 | 0.038 | 72.8 | 0.000870 | 1.66 | 18.99 | 0.20 | 0.0663 | 0.0017 | 0.0518 | 0.0005 | 325.5 | 3.4 |
| 6.2 | c | 248 | 78 | 0.314 | 12.3 | – | <0.01 | 17.29 | 0.20 | 0.0525 | 0.0007 | 0.0579 | 0.0007 | 363.1 | 4.2 |
| 7.1 | c | 154 | 54 | 0.351 | 7.3 | 0.000026 | 0.13 | 18.10 | 0.23 | 0.0544 | 0.0008 | 0.0552 | 0.0007 | 346.2 | 4.3 |
| 8.1 | c | 395 | 100 | 0.253 | 18.4 | 0.000047 | 0.06 | 18.42 | 0.20 | 0.0538 | 0.0 | | | | |

Table 1 (continued)

| Grain spot | U (ppm) | Th (ppm) | Th/U | $^{206}\text{Pb}^*$ (ppm) | $^{204}\text{Pb}/^{206}\text{Pb}$ | f_{206} % | $\frac{^{238}\text{U}}{^{206}\text{Pb}}$ | Total \pm | $^{206}\text{Pb}/^{238}\text{U}$ | Radiogenic \pm | Age (Ma) |
|--|---------|----------|------|---------------------------|-----------------------------------|-------------|--|-----------------------------------|----------------------------------|----------------------------------|----------|
| | | | | | | | \pm | $^{207}\text{Pb}/^{206}\text{Pb}$ | \pm | $^{206}\text{Pb}/^{238}\text{U}$ | \pm |
| <i>C6-AW86-1</i> | | | | | | | | | | | |
| 14.1 | r | 1312 | 23 | 0.017 | 63.7 | 0.000175 | 0.41 | 17.70 | 0.18 | 0.0569 | 0.0004 |
| 14.2 | c | 511 | 197 | 0.385 | 25.8 | – | <0.01 | 17.01 | 0.18 | 0.0532 | 0.0004 |
| 15.1 | c | 783 | 485 | 0.620 | 38.3 | 0.000014 | 0.14 | 17.58 | 0.18 | 0.0548 | 0.0004 |
| Note: Error in Temora reference zircon calibration was 0.34% for the analytical session. | | | | | | | | | | | |

Notes pertaining to all analyses:

1. Uncertainties given at the one σ level.
2. Error in Temora reference zircon calibration not included in above errors but required when comparing data from different mounts.
3. f_{206} % denotes the percentage of ^{206}Pb that is common Pb.
4. Correction for common Pb for the U/Pb data has been made using the measured $^{238}\text{U}/^{206}\text{Pb}$ and $^{207}\text{Pb}/^{206}\text{Pb}$ ratios following Tera and Wasserburg (1972) as outlined in Williams (1998). Correction for common Pb used the measured $^{238}\text{U}/^{206}\text{Pb}$ and $^{207}\text{Pb}/^{206}\text{Pb}$ ratios following Tera and Wasserburg (1972) as outlined in Williams (1998).

Richardson (three samples from two sites: M5-G175; M5-R136A and M5-R136C), and orthoclase-porphyritic gray biotite monzogranite that forms laterally continuous tabular bodies within the layered plutonic association in the southwest part of Mt. Iphigene, bordering Ochs Glacier (C5-Is51A) (for locations, see Fig. 2). The study samples are minimally (sample M5-G175) to substantially (sample M5-R136A, M5-R136C, and; C5-Is51A) affected by migmatization. The aim of investigation of these three samples was to determine a crystallization age for the granitoid phases hypothesized to be part of the Ford Granodiorite in the Ford Ranges (Pankhurst et al., 1998).

Analyses from sample M5-R136A granodiorite and M5-R136C leucosome (a 10-cm thick concordant layer) are combined for an age determination since both samples come from a 1 m² outcrop. Zircon separates from the two constituents were prepared and analyzed separately. The granodiorite plutons underwent solid state deformation within the South Fosdick detachment zone, a normal-oblique shear zone that is in part responsible for the Cretaceous exhumation of the Fosdick complex (McFadden et al., 2007).

Sample C5-Is51A monzogranite exhibits foliation defined by aligned biotite that is deformed by decimeter-scale asymmetric folds. The long limbs of folds host cm-scale leucosomes within diffuse shear bands.

Four granites that occupy discordant dilational structures also were sampled, with the intention of acquiring a lower age bracket on migmatization. The structures that host granite cut across foliation in the granodiorite and the layered plutonic association. Sample C5-I26 is porphyritic cordierite leucogranite in an irregular discordant band that cuts foliation in migmatitic granodiorite orthogneiss, and truncates weak magmatic layering and schlieren in leucogranite (Fig. 5d). The sample is unfoliated and contains cm-sized sub- to euhedral K-feldspar and cordierite. In thin section, cordierite and K-feldspar have sub- to euhedral crystal faces with optically uniform quartz in interstices and along grain boundaries (cf. Fig. 5a, b). These microstructures are indicative of crystallization of the leucogranite from melt (e.g. Holness and Sawyer, 2008). A second granite sample comes from a two-meter thick discordant sill within the residual paragneiss domain at Mt. Avers. The rock is a white K-feldspar granite with a weak foliation defined by sparse biotites (C6-AW86-1). The third sample is a leucogranite (C5-Mj70SB) that fills meters-scale normal-sense shear bands cutting the intermediate to mafic metaplutonic rocks of the layered plutonic association (Fig. 4a). The fourth and final sample is leucogranite from a 30-cm thick discordant dike (M5-F100) (Fig. 5e) that is one within an undeformed tensile array cutting at a high angle across migmatite structures in gneisses at Mt. Ferranto. The crosscutting relationship and lack of deformation of the array suggest that the dike age should provide a lower limit on the time of migmatization and deformation of host gneisses.

3.3. Results

U, Pb, and Th results are presented in Table 1 and REE data appear in Table 2. Graphical representations of the data in Tera-Wasserburg diagrams and histograms are in Figs. 7 and 8. Where used in the text,

the term *core* refers to the innermost part of a zircon grain with coherent cathodoluminescence (CL) characteristics, and *rim* is used for surrounding material with contrasting CL properties. The identifiers “c” for core and “r” for rim for individual analysis spots appear in Column 2, Table 1.

3.3.1. Th/U ratios

The majority of Devon-Carboniferous zircons have U and Th concentrations in the range of 100–2200 and 0–560 ppm, respectively (Table 1). Th/U values fall into two groups. Relatively high Th/U ratios in the range of 0.31 to 0.78 (47% of analysed grains) correspond to zircon cores, with the highest ratios >0.5 measured in acicular, igneous grains with oscillatory zoning. The values are in the typical or normal range for igneous grains crystallized from a magma. Rim overgrowths (dark in CL, comprising 48% of analyses) have comparatively low Th/U values in the range of 0.023 to 0.15, consistent with metamorphic origin (Williams and Claesson, 1987). However it should be noted that in some cases, low Th/U ratios in zircons arise from an enrichment in U interpreted to be due to zircon crystallizing from a U-enriched partial melt phase.

3.3.2. Cathodoluminescence characteristics and U–Pb geochronology

3.3.2.1. Ford Granodiorite. The majority of zircons in sample M5-G175 have bright, unzoned or medium dark, oscillatory zoned euhedral grains with rims of irregular width (Fig. 6a). Rims are uniformly dark in CL and have Th/U ratios mostly less than 0.012. From the 18 analyses of 16 grains a weighted mean age of 369.2 ± 2.5 Ma is calculated for the dominant group of 10 analyses (MSWD = 1.14). This gives the crystallization age of granodiorite at Mt. Getz (Fig. 7a, b).

The granodiorite sample from Mt. Richardson combines zircons from the granodiorite host, M5-R136A, with zircons having matching characteristics from a concordant leucogranite layer within the granodiorite, sample M5-R136C. The population consists of euhedral blocky zircons with bipyramidal terminations, 100–300 μm in length, with a 2:1 axial ratio (Fig. 9). In CL images, oscillatory zoning is evident in entire crystals or within wide rims upon a core with contrasting CL characteristics. The zircons of this population that come from the leucosome portion of the sample are considered to be xenocrysts from the host/source granodiorite portion, and so the mean age was calculated using data from both samples. Nine of 11 cores and 3 rims yield Devonian ages (Table 1) that give a weighted mean age of 366.6 ± 4.2 Ma ($n = 12$, MSWD = 2.2) (Fig. 7c, d).

Sample C5-Is51A, the porphyritic grey biotite monzogranite, has a prevalent zircon population consisting of doubly terminated, prismatic, acicular igneous grains that have pronounced, fine-scale oscillatory zoning in CL (Fig. 6b). In transmitted light, the zircons are very clear and inclusion free. Six core analyses of primary magmatic grains and 2 analyses of dark rim overgrowths, the latter with low Th/U due to high U (*circa* 2335 and 1670 ppm respectively) give a weighted mean $^{238}\text{U}/^{206}\text{Pb}$ age of 353.4 ± 3.2 Ma ($n = 8$,

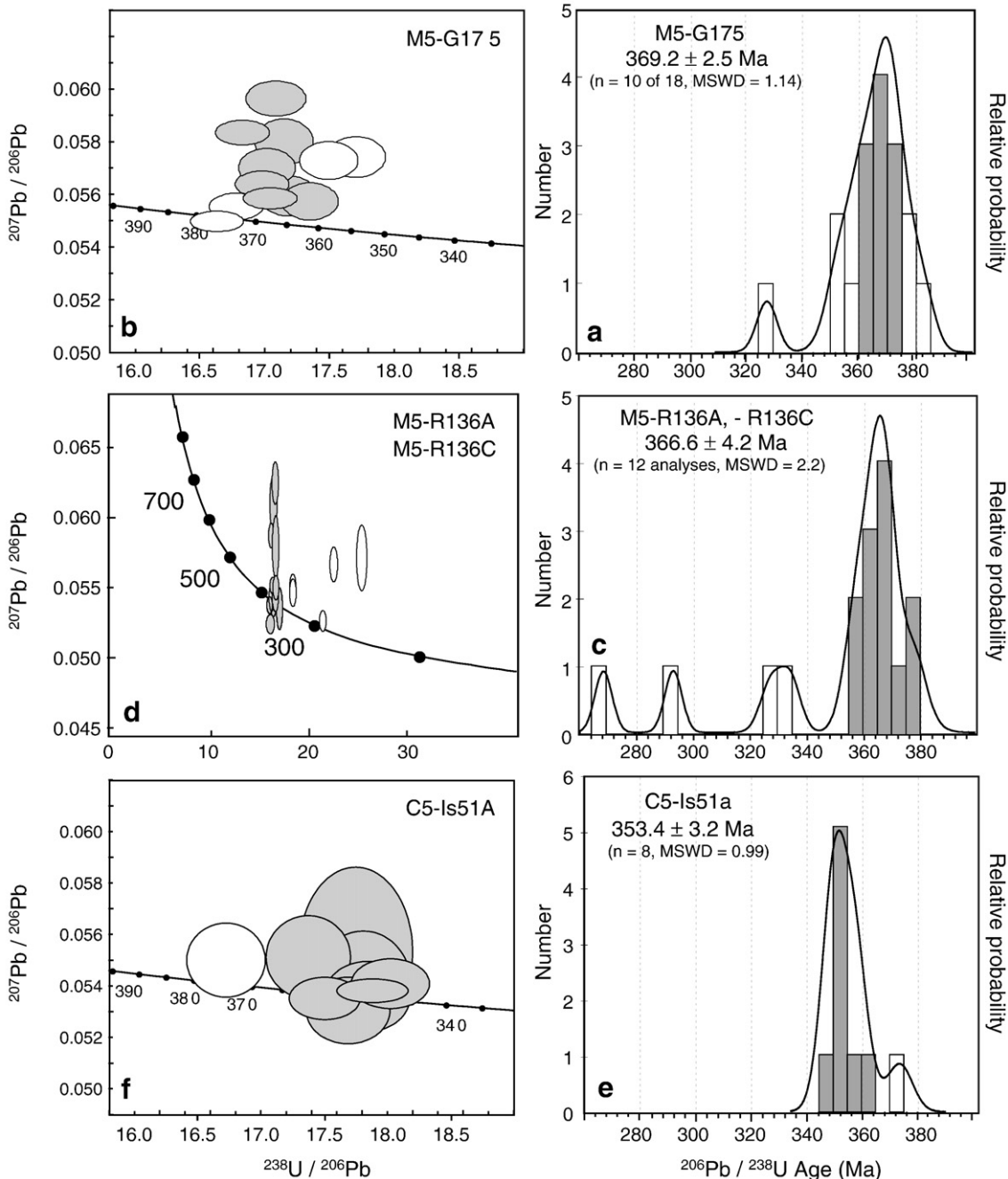


Fig. 7. Tera-Wassburg concordia diagrams and relative probability plots with stacked histograms for granodiorite and monzogranite samples. Data-point error ellipses on concordia diagrams are at 68.3% confidence. a–b. Sample M5-G175 from the Ford suite granodiorite pluton at Mt. Getz. c–d. Samples M5-R136A and M5-R136C from the Ford suite granodiorite pluton at Mt. Richardson. e–f. Sample C5-Is51a from porphyritic monzogranite orthogneiss of Mt. Iphigene.

MSWD = 0.99; Fig. 7e, f). This is interpreted as the crystallization age of primary magmatic zircon within the original plutonic rock. Four analyses yield Cambrian or older ages for cores identifiable in CL.

3.3.2.2. Leucogranites. The crosscutting dike at Mt. Ferranto, M5-F100, contains zircon that has moderately dark, zoned cores with wide dark rims. The rims are 20 to 40 μm wide, and lack zoning under CL. All but two of the SHRIMP analysis spots are within rims. Six analyses yield a weighted mean age of 368.1 ± 6.3 Ma (MSWD = 1.8; Fig. 8a, b).

The porphyritic granite, C5-I26, contains a dominant zircon population that consists of clear, bipyramidal, elongate zircon grains with oscillatory zoning evident under CL (Fig. 6c). Fourteen of sixteen analyses of cores and rims combine for a weighted mean age of $364.4 \pm$

2.5 Ma (MSWD = 1.06; Fig. 8c, d). A thin high U rim (dark in CL, ~3 μm in width) was too narrow to be analysed.

Zircons extracted from leucogranite of sample C5-Mj70SB, from in extensional shear bands at Marujupu Peak (Fig. 4), have cores that are low in U, bright under CL. Truncations of sector and oscillatory zoning in the cores against rim overgrowths suggest that the cores are xenocrystic or inherited, probably from a plutonic host. Uniform rims, dark in CL and 20 to 40 μm wide, are evident on almost all grains. All of the SHRIMP analysis spots are within the rims (Table 1). Four analyses form a bimodal grouping at about 355–365 Ma (Fig. 8e, f).

The concordant sill within migmatitic paragneisses at Mt. Avers, sample C6-AW86-1, has a dominant population of subhedral, elongate, moderately dark, zoned zircons with medium gray rims. The weighted

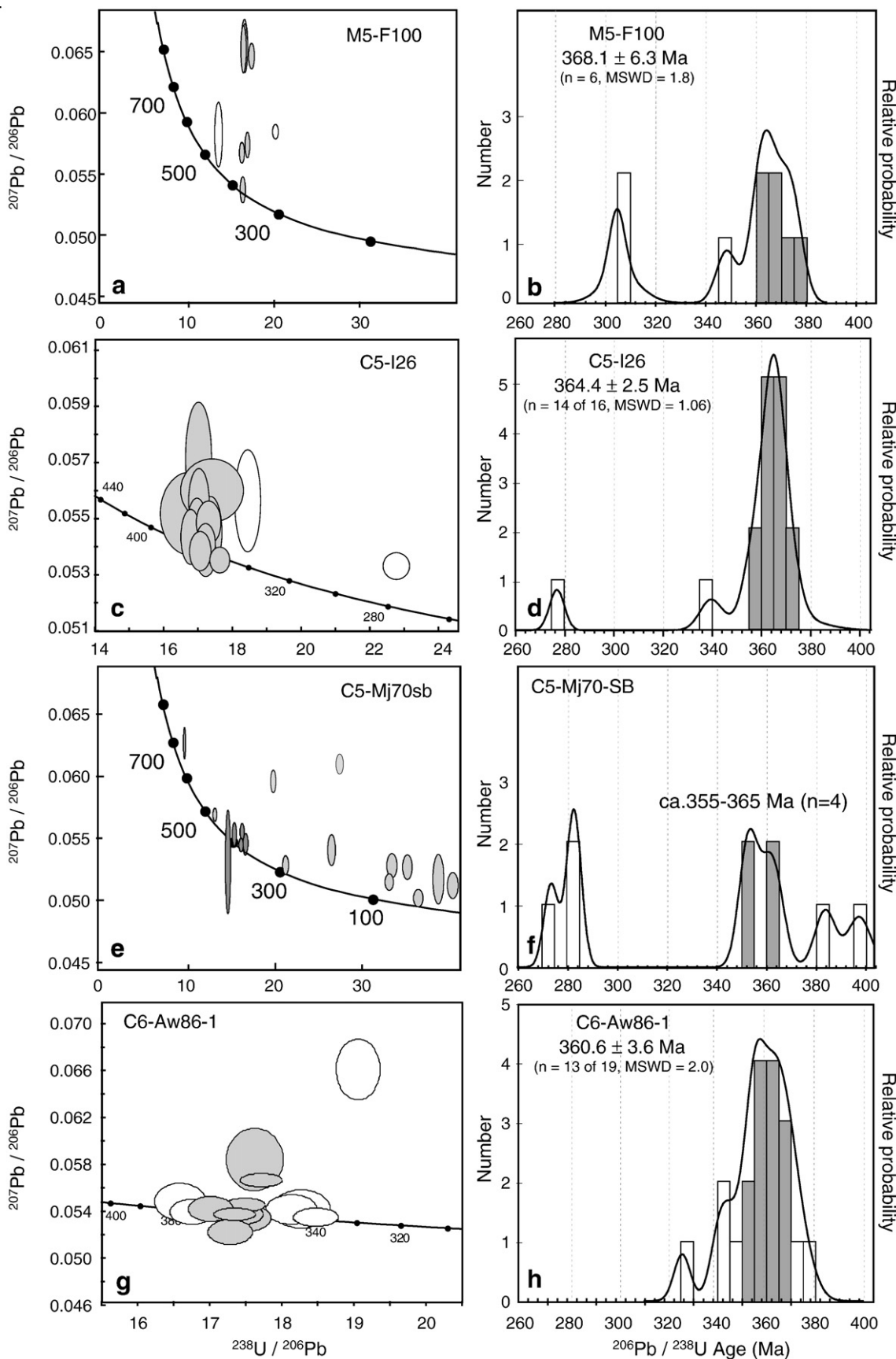


Fig. 8. Tera-Wasserburg concordia diagrams and relative probability plots with stacked histograms for leucogranite samples. Data-point error ellipses on concordia diagrams are at 68.3% confidence. a–b. Sample M5-F100 from a discordant granite cutting migmatite gneisses at Mt. Ferranto. c–d. Sample C5-I26 from cordierite granite body cutting the layered plutonic association at Mt. Iphigene. e–f. Sample C5-Mj70SB, granite emplaced in extensional shear bands cutting layered plutonic association at Marujupu Peak. g–h. Sample C6-Aw86-1, garnet-K-feldspar granite from a concordant sill within paragneiss at western Mt. Avers.

Table 2

REE and trace element data for two Devonian zircons (SHRIMP RG) from the dominant population in sample M5-R136A.

| Spot | La | Ce | Pr | Nd | Sm | Eu | Gd | Tb | Dy | Ho | Er | Tm | Yb | Lu | Y | Hf |
|------|-------|-------|-------|-------|-------|-------|-------|-------|-------|-------|-------|-------|--------|-------|--------|-------|
| 4.1 | 0.004 | 20.41 | 0.045 | 0.929 | 2.452 | 0.501 | 14.85 | 6.465 | 88.03 | 38.93 | 198.0 | 48.47 | 506.0 | 110.6 | 1299 | 14089 |
| 4.1 | | | | 0.954 | 2.413 | 0.459 | 15.21 | | 91.45 | | 195.0 | | 517.0 | | | 14263 |
| 25.1 | 0.052 | 31.79 | 0.495 | 7.79 | 12.44 | 2.07 | 56.79 | 21.84 | 267.2 | 105.5 | 488.1 | 109.9 | 1008.0 | 201.5 | 3845.7 | 11819 |
| 25.1 | | | | 7.45 | 12.22 | 2.21 | 56.62 | | 267.9 | | 484.5 | | 1028.7 | | | 11892 |

Weight %.

Analysed against standard glass NIST611.

Zircon, isotope $\mu\text{ml/g}$: 153.186813.

All REE and Y concentrations are in ppm.

Zircon isotope ppm, 13,940.

mean age calculated from 13 of the 19 Paleozoic analyses of rims and cores is 360.6 ± 3.6 Ma (MSWD = 2.0; Fig. 8g, h).

3.3.3. REE for sample M5-R136A (Ford Granodiorite)

Rare earth element data for two zircons of the same igneous population are reported in Table 2 and normalized to chondrite in Fig. 9. The patterns from both core and rim analysis are similar, although core concentrations are higher, with both showing steeply rising slopes from light REE to heavy REE with positive Ce and negative Eu anomalies. The values are in the range of those for typical crustal zircons (Hoskin and Schaltegger, 2003). From the two data available, it appears that REE systematics were stable and unaffected by changes in melt composition

during zircon growth. There are insufficient data to detect effects of feldspar fractionation on zircon or to recognize replenishment of melt through a permeability network of framework grains.

4. Discussion

While it has been recognized that multiple HT events affected the Fosdick Mountains migmatite–granite complex (Korhonen et al., 2007; Saito et al., 2007a,b; Korhonen et al., 2008), up until now there has been only limited geochronology to aid interpretation of the principal plutonic and tectonometamorphic events. The degree and significance of Paleozoic metamorphism, as distinct from Cretaceous activity related to

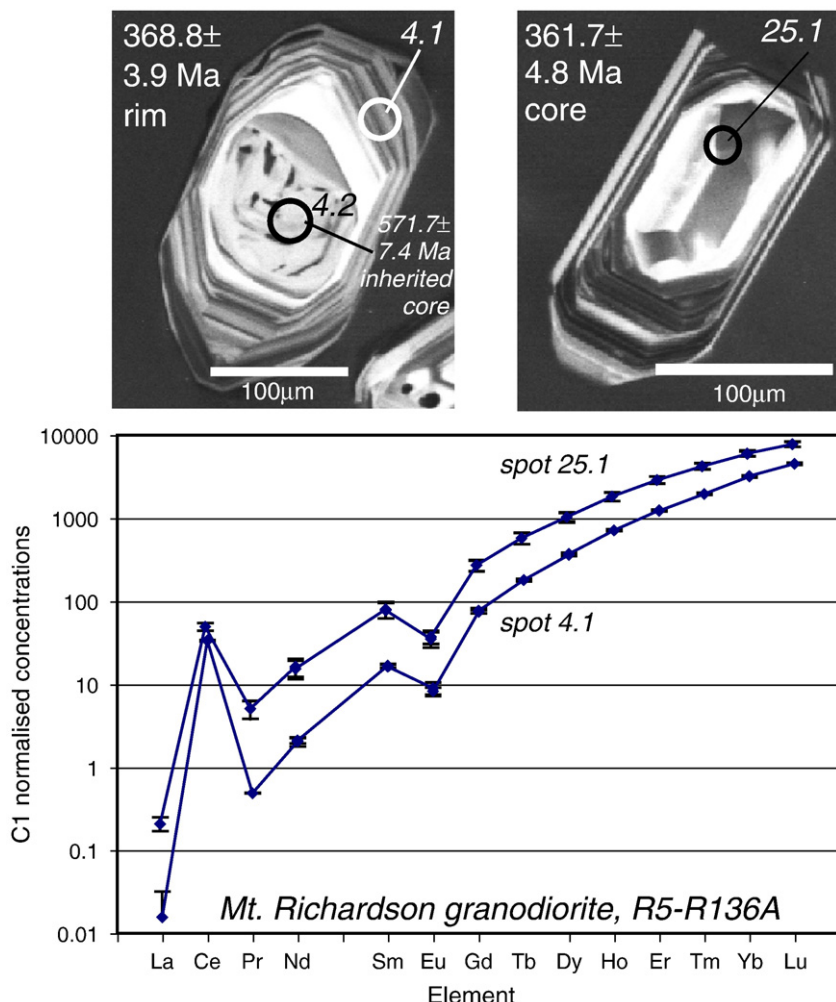


Fig. 9. Rare earth element (REE) data for two igneous grains from the dominant zircon population of Ford Granodiorite sample M5-R136A. Data are provided in Table 2. Plot is normalized to chondrite. Similar patterns from both core and rim have steeply rising slopes from light REE to heavy REE, with positive Ce and negative Eu anomalies. Values are in the typical range for crustal zircons (Hoskin and Schaltegger, 2003). Grain 4 has a rounded core that likely originated as a detrital grain in a Swanson Formation source.

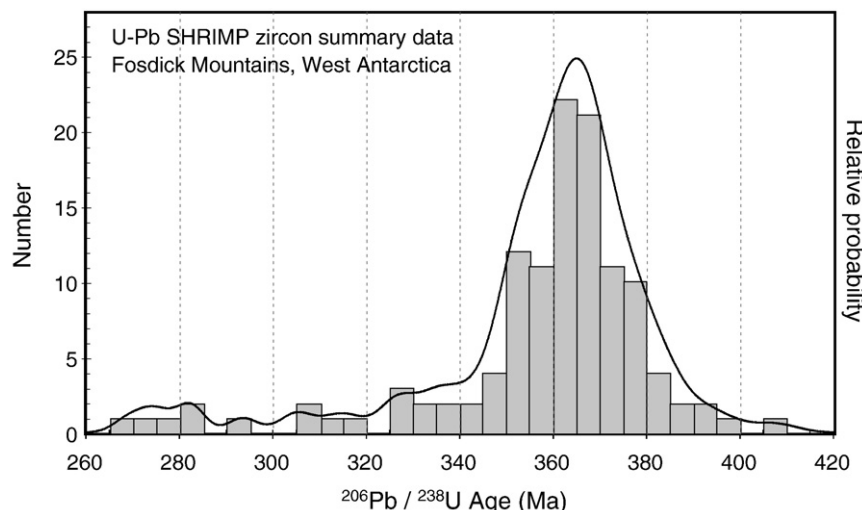


Fig. 10. Relative probability plot with stacked histogram compilation and summary of the Paleozoic U-Pb SHRIMP zircon ages for Fosdick Mountains samples reported here and in Siddoway et al. (2004; sample 01222-B10).

the West Antarctic rift system (McFadden et al., 2007; Siddoway, 2008) were unclear. Our new U-Pb SHRIMP zircon results identify a magmatic interval spanning 380 to 350 Ma, with a peak at 365 Ma, summarized on the relative probability plot with stacked histogram in Fig. 10. Results from granodiorites of the Fosdick Mountains are *circa* 369 Ma and 366 Ma (Fig. 7), within the range of ages for Ford Granodiorite obtained by Pankhurst et al. (1998) for mesozonal granodiorite plutons of the Ford Ranges. We view the result as a substantiation of the hypothesis that Ford Granodiorite is an integral component of the Fosdick Mountains migmatite–granite complex (cf. Siddoway et al., 2004).

The 368 to 365 Ma ages for three granites (Fig. 8) overlap or are very close to the granodiorite ages. The granites occupy structures that cut migmatitic layering within the layered plutonic association (Figs. 4a, 5d–e), a relationship that suggests sustained elevated temperatures in the middle to deep crust during convergent margin magmatism. Deformation imparted a subhorizontal migmatitic foliation, indicating vertical shortening, and an array of extensional shear bands shows NNE–SSW stretching, in accordance with mineral lineation and AMS stretching axis (Fig. 4). The direction is approximately opposite to the direction of Paleozoic convergence upon East Gondwana's active margin (Fig. 1).

The youngest samples from the Fosdick Mountains are a sill of leucogranite hosted by paragneiss that is inferred to be meta-Swanson Formation, and sheet-like body of monzogranite within the plutonic association. Their ages are *circa* 359 Ma and 353 Ma, respectively (Fig. 8e–h). The monzogranite sample is noted to contain inherited zircon with Cambrian and older ages (Fig. 6b) that appear to fit the characteristic pattern of Ross Orogen-derived detrital grains of the Swanson Formation (Ireland et al., 1998; Siddoway et al., 2004). Geochemical investigation of sample C5-Is51A by Saito et al. (2007a,b) identifies the granite as having geochemical and isotope characteristics that indicate derivation from partial melting of Swanson Formation or a comparable sedimentary source. A possible explanation for the notably younger age for the C5-Is51A granite is that emplacement of crustally-derived melts lagged behind calc-alkaline magmatism related to Gondwana convergent margin processes. The two-mica granites in the region that have U-Pb monazite ages of *circa* 359 and 351 Ma (Tulloch et al., 2009) lend support to this trend.

The NNE–SSW stretching direction obtained from mesoscopic structures and anisotropy of magnetic susceptibility fabrics (Fig. 4) is distinct from the N 50 E to N 75 E trend documented for Cretaceous transtension (Siddoway, 2008) and normal-oblique translation on the South Fosdick detachment fault (McFadden et al., 2007). Potentially the kinematics of mesoscopic structures that host Paleozoic granite are

evidence of NNE–SSW extension, generally orthogonal to the Gondwana margin, affecting the Paleozoic intermediate plutonic rocks soon after their emplacement at 369–366 Ma. The extensional structures overprinting the plutonic complex provide a possible indication that the elevated temperatures were a consequence of lithospheric thinning. Microstructures in the granites (Fig. 5a–c) including zircon morphological characteristics such as doubly terminated prismatic grains (Fig. 6) indicate that melt was present during deformation and thus elevated temperatures accompanied the deformation. The microstructures are in accord with determinations of $T > 800$ °C at depths of 23 to 33 km (Korhonen et al., 2008), conditions suitable to cause extensive melting.

The new U-Pb zircon ages for migmatite and anatetic granite of the Fosdick Mountains, representing the middle to deep crust in the West Antarctic sector of the East Gondwana active margin, are contemporaneous with those for plutonic rocks of the western and central Lachlan belt (Ireland et al., 1998; Foster and Gray, 2000; Black et al., 2005; Kemp et al., 2007) and with the Western Province of New Zealand at 371 to 358 Ma (Kimbrough et al., 1993; Muir et al., 1996; Tulloch et al., 2009) (Fig. 11). The results indicate that HT metamorphism and crustal melting were contemporaneous and widespread along much of the East Gondwana margin in Late Devonian to Carboniferous time. The U-Pb zircon ages fall within a 15 to 20 million year interval, suggesting an event of fairly short duration. A dramatic silicic phase of magmatism in the Karamea Batholith occurred over an even shorter time interval between 371 and 368 Ma, according to recent work by Tulloch et al. (2009).

The granites that occupy dilational structural sites in the Fosdick Mountains are considered to be formed during migration of anatetic melts produced during high temperature metamorphism, according to structural context and preliminary geochemistry. Future research must establish whether the melt migration and emplacement occurred during the well-documented convergence on the East Gondwana margin (Bradshaw et al., 1983; Weaver et al., 1991; Adams, 2004) or post-tectonic extension which is less certain (Pankhurst et al., 1998; Bradshaw, 2007). The presence of Paleozoic extensional structures in the middle to deep crust could offer a potential resolution to some recent perplexities in Marie Byrd Land tectonics. For example, Pankhurst et al. (1998) discovered that exposures of metasedimentary migmatites of the Alexandra Mountains (location, Fig. 2) have distinctly different protoliths than the Fosdick migmatites. The Alexandra Mountains paragneisses contain a dominant inherited zircon population with ages in the range of 400–320 Ma, an indication that the protolith contained detritus eroded

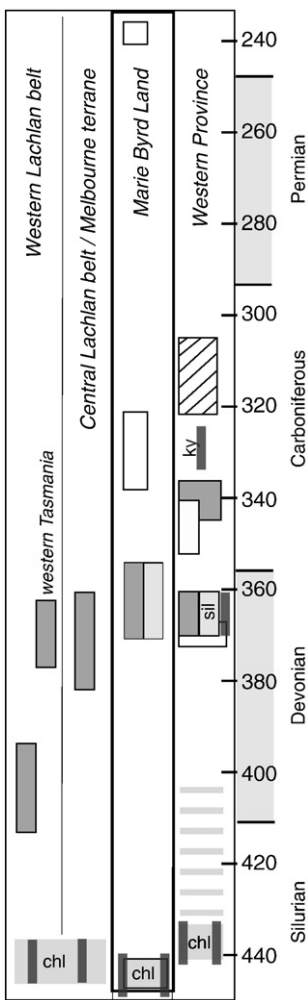


Fig. 11. Comparison of the range of U-Pb SHRIMP ages for the Fosdick Mountains, Marie Byrd Land (3rd column) versus U-Pb age ranges from parts of the Lachlan Orogen, Australia, and the Western Province, New Zealand. Calc-alkaline phases are in grey, peraluminous (or low Sr) granites are in white, and alkalic granites are in black. Metamorphic intervals are indicated by the bar symbol associated with a mineral phase: chl, chlorite; st, staurolite; and ky, kyanite. Sources are as follows: Lachlan belt—Foster and Gray (2000), Kemp et al. (2007); Tasmania—Black et al. (2005); New Zealand—Tulloch et al. (2009), Ireland and Gibson (1998), Muir et al. (1996), Kimbrough et al. (1993); Marie Byrd Land—this study and Siddoway et al. (2004).

from Ford Granodiorite and Devono-Carboniferous granitoids of the region. The paragneiss may have originated as sedimentary rocks deposited in a Permo-Triassic successor basin formed during transient late Paleozoic extension (Pankhurst et al., 1998), that later underwent tectonic burial and HT metamorphism in Jurassic–Cretaceous time.

A second enigma is the presence of isolated “exotic” outliers of Delamerian–Ross-type crust far to the east of their expected positions on the East Gondwana margin (Bradshaw, 2007) (Fig. 1). Two of these tectonic entities are the Takaka terrane in New Zealand and an isolated basement exposure in eastern Marie Byrd Land (Fig. 1), both of which contain igneous and metamorphic rocks that have isotopic characteristics and ages matching the signature of the Ross Orogen (Pankhurst et al., 1998; Gutjahr et al., 2006). The pre-breakup configuration of East Gondwana places them distant (>1000 km; Fig. 1) from their place of origin in the Delamerian–Ross Orogen. Bradshaw (2007) postulates that they may be rifted fragments excised from the Delamerian–Ross orogen by dramatic post-Cambrian extension. There is a growing recognition that the overall convergent tectonics that brought about the Paleozoic growth and stabilization of the wide proto-Pacific margin of Gondwana was interrupted by periods of crustal extension (Foster and Gray, 2000; Crawford et al., 2003; Gray and Foster, 2004) induced by subduction

zone retreat (Collins, 2002), that could have been responsible for excision of the tectonic slivers in Paleozoic time. During these periods, dramatic thinning of the lithosphere brought hot asthenosphere into closer proximity to the crust, causing high heat flow, HTLP metamorphism, and crustal melting (Foster and Gray, 2000; Collins, 2002). The U-Pb SHRIMP zircon ages of Ford Granodiorite plutonic phases, monzogranites derived from melting of supracrustal sedimentary rocks, and anatetic granites emplaced in extensional structures in the Fosdick Mountains suggest that these margin-wide processes affected West Antarctica and that the tectonism coincided in time (Fig. 11) with events in the central Lachlan belt of Australia and the South Island of New Zealand.

Acknowledgments

Foremost we thank Rory McFadden for his substantial contributions to this work in the field and laboratory. P. Rey and an anonymous reviewer provided helpful reviews, together with M. Brown, R. McFadden, F. Korhonen, and S. Saito who gave input on an earlier manuscript. Fruitful collaborations in the field involved F. Korhonen, C. Teyssier, and S. Kruckenberg. Contributions to the SHRIMP research came from S. Fadrhonc, C. McGee, S. Mertens and B. Armstrong. Field support from M. Roberts, A. O'Bannon, F. McCarthy, J. Haffey, Raytheon Polar Services, and Kenn Borek Air made the sample acquisition possible. The work was carried out under U.S. National Science Foundation research grant OPP-0338279.

References

- Adams, C.J., 1986. Geochronological studies of the Swanson Formation of Marie Byrd Land, West Antarctica, and correlation with northern Victoria Land, East Antarctica, and South Island, New Zealand. *New Zealand Journal of Geology and Geophysics* 29, 354–358.
- Adams, C.J., 2004. Rb-Sr age and strontium isotopic characteristics of the Greenland Group, Buller terrane, New Zealand, and correlations at the East Gondwana margin. *New Zealand Journal of Geology and Geophysics* 47, 189–200.
- Berry, R.F., Steele, D.A., Meffre, S., 2008. Proterozoic metamorphism in Tasmania: implications for tectonic reconstructions. *Precambrian Research* 166 (1–4), 387–396.
- Black, L.P., Kamo, S.L., Allen, C.M., Aleinikoff, J.N., Davis, D.W., Korsch, R.J., Foudoulis, C., 2003. TEMORA 1: a new zircon standard for Phanerozoic U-Pb geochronology. *Chemical Geology* 200, 155–170.
- Black, L.P., McClenaghan, M.P., Korsch, R.J., Everard, J.L., Foudoulis, C., 2005. Significance of Devonian–Carboniferous igneous activity in Tasmania as derived from U-Pb SHRIMP dating of zircon. *Australian Journal of Earth Sciences* 52 (6), 807–829.
- Bons, P.D., Druguet, E., Castaño, L.M., Elburg, M.A., 2008. Finding what is now not there anymore: recognizing missing fluid and magma volumes. *Geology* 36, 851–854.
- Bradshaw, J.D., 2007. The Ross Orogen and Lachlan Fold Belt in Marie Byrd Land, Northern Victoria Land and New Zealand: Implication for the tectonic setting of the Lachlan Fold Belt in Antarctica. In: Cooper, A.K., Raymond, C., et al. (Eds.), *Antarctica: A Keystone in a Changing World – Online Proceedings of the 10th ISAES*. U.S. Geological Survey and The National Academies. <http://pubs.usgs.gov/of/2007/1047/srp/srp059>.
- Bradshaw, J.D., Andrew, P.B., Field, B.D., 1983. Swanson Formation and related rocks of Marie Byrd Land and a comparison with the Robertson Bay Group of northern Victoria Land. In: Oliver, R.L., James, P.R., Jago, J.B. (Eds.), *Antarctic Earth Science*. Australian Academy of Science, Canberra, pp. 274–279.
- Chappell, B.W., White, A.J.R., 1992. I- and S-type granites in the Lachlan Fold Belt. *Transactions of the Royal Society of Edinburgh* 83 (1–2), 1–26.
- Collins, W.J., 2002. Nature of extensional accretionary orogens. *Tectonics* 21, 1024.
- Collins, W.J., Hobbs, B.E., 2001. What caused the Early Silurian change from mafic to silicic (S-type) magmatism in the eastern Lachlan Fold Belt? *Australian Journal of Earth Sciences* 48, 25–41.
- Coney, P.J., 1992. The Lachlan belt of eastern Australia and Circum-Pacific tectonic evolution. *Tectonophysics* 214, 1–25.
- Crawford, A.J., Meffre, S., Symonds, P.A., 2003. 120 to 0 Ma tectonic evolution of the southwest Pacific and analogous geological evolution of the 600 to 220 Ma Tasman Fold Belt System. *Geological Society of Australia Special Publication*, vol. 22, pp. 377–397.
- Fergusson, C.L., Coney, P.J., 1992. Implications of a Bengal fan-type deposit in the Paleozoic Lachlan fold belt of southeastern Australia. *Geology* 20, 1047–1049.
- Flöttmann, T., Gibson, G.M., Kleinschmidt, G., 1993. Structural continuity of the Ross and Delamerian orogens of Antarctica and Australia along the margin of the paleo-Pacific. *Geology* 21 (4), 319–322.
- Foster, D., Gray, D., 2000. Evolution and structure of the Lachlan Fold Belt (Orogen) of Eastern Australia. *Annual Review of Earth and Planetary Sciences* 28, 47–80.

- Foster, D.A., Gray, D.R., Bucher, M., 1999. Chronology of deformation within the turbidite-dominated Lachlan orogen: implications for the tectonic evolution of eastern Australia and Gondwana. *Tectonics* 18. doi:10.1029/1998TC900031.
- Glen, R.A., 2005. The Tasmanides of eastern Australia. Special Publication, vol. 246. Geological Society, London, pp. 23–96.
- Gray, D.R., Foster, D.A., 1998. Character and kinematics of faults within the turbidite-dominated Lachlan Orogen: implications for tectonic evolution of eastern Australia. *Journal of Structural Geology* 20 (12), 1691–1720.
- Gray, D.R., Foster, D.A., 2004. Tectonic evolution of the Lachlan Orogen, southeast Australia: historical review, data synthesis and modern perspectives. *Australian Journal of Earth Sciences* 47, 772–817.
- Gray, D., Foster, D.A., Bucher, M., 1997. Recognition and definition of orogenic events in the Lachlan Fold Belt. *Australian Journal of Earth Sciences* 44, 489–501.
- Guo, J., O'Reilly, S.Y., Griffin, W.L., 1996. Zircon inclusions in corundum megacrysts: I. Trace element geochemistry and clues to the origin of corundum megacrysts in alkali basalts. *Geochimica et Cosmochimica Acta* 60 (13), 2347–2363.
- Gutjahr, M., Bradshaw, J.D., Weaver, S., Münke, C., Ireland, T., 2006. Provenance of Cambrian conglomerates from New Zealand: implications for the tectonomagmatic evolution of the SE Gondwana margin. *Journal of the Geological Society* 163, 997–1010.
- Harrison, T.M., Watson, E.B., Aikman, A.B., 2007. Temperature spectra of zircon crystallization in plutonic rocks. *Geology* 35 (7), 635–638.
- Hawkesworth, C.J., Kemp, A.I.S., 2006. Using hafnium and oxygen isotopes in zircons to unravel the record of crustal evolution. *Chemical Geology* 226, 144–162.
- Holness, M.B., Sawyer, E.W., 2008. On the pseudomorphing of melt-filled pores during the crystallization of migmatites. *Journal of Petrology* 49, 1343–1363.
- Hoskin, P.W.O., 1998. Minor and trace element analysis of natural zircon ($ZrSiO_4$) by SIMS and laser ablation ICPMS: a consideration and comparison of two broadly competitive techniques. *Journal of Trace and Microprobe Techniques* 16, 301–326.
- Hoskin, P.W.O., Schaltegger, U., 2003. The composition of zircon and igneous and metamorphic petrogenesis. *Reviews in Mineralogy & Geochemistry* 51 (1), 27–62.
- Ireland, T.R., Wlotzka, F., 1992. The oldest zircons in the solar system. *Earth and Planetary Science Letters* 109 (1–2), 1–10.
- Ireland, T.R., Gibson, G.M., 1998. SHRIMP monazite and zircon geochronology of high-grade metamorphism in New Zealand. *Journal of Metamorphic Geology* 16, 149–167.
- Ireland, T.R., Flöttmann, T., Fanning, C.M., Gibson, G.M., Preiss, V.W., 1998. Development of the early Paleozoic Pacific margin of Gondwana from detrital-zircon ages across the Delamerian orogen. *Geology* 26, 243–246.
- Jenkins, R.B., Landenberger, B., Collins, W.J., 2002. Late Palaeozoic retreating and advancing subduction boundary in the New England Fold Belt, New South Wales. *Australian Journal of Earth Sciences* 49, 467–489.
- Kemp, A.I.S., Hawkesworth, C.J., Foster, G.L., Paterson, B.A., Woodhead, J.D., Hergt, J.M., Gray, C.M., Whitehouse, M.J., 2007. Magmatic and crustal differentiation history of granitoid rocks from Hf–O isotopes in zircon. *Science* 315, 980–983.
- Kimbrough, D.L., Tulloch, A.J., Geary, A., Coombs, D.S., Landis, C.A., 1993. Isotopic ages from the Nelson region of South Island, New Zealand: crustal structure and definition of the Median Tectonic zone. *Tectonophysics* 225 (4), 433–448.
- Korhonen, F.J., Brown, M., Siddoway, C.S., 2007. Petrologic and geochronological constraints on the polymetamorphic evolution of the Fosdick migmatite dome, Marie Byrd Land, West Antarctica. In: Cooper, A.K., Raymond, C., et al. (Eds.), *Antarctica: A Keystone in a Changing World – Online Proceedings and Conference Abstracts*. USGS OFR-2007-1047. http://pubs.usgs.gov/of/2007/1047/ea/of2007-1047ea049.pdf.
- Korhonen, F.J., Brown, M., Saito, S., Siddoway, C.S., 2008. The link between migmatites and granites: polyphase melting and granite magmatism during the tectonic evolution of the Fosdick migmatite dome, West Antarctica. 33rd International Geologic Congress, Oslo, Norway. Abstract MPN12812L.
- Kretz, R., 1983. Symbols for rock-forming minerals. *American Mineralogist* 68 (1–2), 277–279.
- Ludwig, K.R., 2001. SQUID 1.02, A User's Manual. Berkeley Geochronology Center Special Publication, vol. 2. 2455 Ridge Road, Berkeley, CA 94709, USA. www.bgc.org/isoplot/etc/Squid1.03Manual.pdf.
- Ludwig, K.R., 2003. User's Manual for Isoplot/Ex, Version 3.0, A geochronological toolkit for Microsoft Excel. vol. 4. Berkeley Geochronology Center Special Publication, 2455 Ridge Road, Berkeley, CA 94709, USA. www.bgc.org/isoplot/etc/Isoplot3betaManual.pdf.
- Maas, R., Kinny, P.D., Williams, I.S., Froude, D.O., Compston, W., 1992. The Earth's oldest known crust: a geochronological and geochemical study of 3900–4200 Ma old detrital zircons from Mt. Narryer and Jack Hills, Western Australia. *Geochimica et Cosmochimica Acta* 56, 1281–1300.
- McFadden, R., Siddoway, C.S., Teyssier, C., Fanning, C.M., Kruckenberg, S.C., 2007. Cretaceous oblique detachment tectonics in the Fosdick Mountains, Marie Byrd Land, Antarctica. In: Cooper, A.K., Raymond, C., et al. (Eds.), *Antarctica: A Keystone in a Changing World – Online Proceedings of the 10th International Symposium on Antarctic Earth Sciences*, USGS OFR-2007-1047. doi:10.3133/of2007-1047.srp046.
- McFadden, R., Teyssier, C., Siddoway, C.S., Fanning, C.M., Kruckenberg, S.C., 2008. Structural and rheological controls of km-scale melt transport and accumulation in a migmatite complex: Fosdick Mountains, West Antarctica. *Geological Association of Canada – Mineralogical Association of Canada Abstracts*, vol. 33, pp. 108–109.
- Muir, R.J., Ireland, T.R., Weaver, S.D., Bradshaw, J.D., 1996. Ion microprobe dating of Paleozoic granitoids: Devonian magmatism in New Zealand and correlations with Australia and Antarctica. *Chemical Geology* 127, 191–210.
- Nathan, S., Rattenbury, M.S., Suggate, R.P. (compilers), 2002. GNS QMAP Geology of the Greymouth area. Institute of Geological and Nuclear Sciences [New Zealand], 1:250 000.
- Pankhurst, R.J., Weaver, S.D., Bradshaw, J.D., Storey, B.C., Ireland, T.R., 1998. Geochronology and geochemistry of pre-Jurassic superterranes in Marie Byrd Land, Antarctica. *Journal of Geophysical Research* 103, 2529–2547.
- Saito, S., Korhonen, F.J., Brown, M., Siddoway, C.S., 2007a. Petrogenesis of granites in the Fosdick migmatite dome, Marie Byrd Land, West Antarctica (extended abstract). In: Cooper, A.K., Raymond, C., et al. (Eds.), *Antarctica: A Keystone in a Changing World – Proceedings and Conference Abstracts Online*. US Geological Survey, USGS OFR-2007-1047. http://pubs.usgs.gov/of/2007/1047/ea/of2007-1047ea105.pdf.
- Saito, S., Brown, M., Korhonen, F.J., Siddoway, C.S., 2007b. Contrasting sources of granites in the Fosdick Migmatite Dome, West Antarctica. Fall Meeting Suppl., Abstract V51C-0723. *Eos Transactions of the American Geophysical Union*, vol. 88(52).
- Sambridge, M.S., Compston, W., 1994. Mixture modeling of multi-component data sets with application to ion-probe zircon ages. *Earth and Planetary Science Letters* 128 (3–4), 373–390.
- Sawyer, E.W., 2008. Working with Migmatites: Nomenclature for the Constituent Parts. In: Sawyer, E.W., Brown, M. (Eds.), *Working with Migmatites*. Mineralogical Association of Canada, vol. 38, pp. 1–28.
- Siddoway, C., 2008. Tectonics of the West Antarctic rift system: new light on the history and dynamics of distributed intracontinental extension. In: Cooper, A.K., Raymond, C., et al. (Eds.), *Antarctica: A Keystone in a Changing World*. National Academy of Sciences, Washington, D.C., pp. 91–114.
- Siddoway, C.S., Richard, S.M., Fanning, C.M., Luyendyk, B.P., 2004. Origin and emplacement of a middle Cretaceous gneiss dome, Fosdick Mountains, West Antarctica. In: Whitney, D.L., Teyssier, C., Siddoway, C.S. (Eds.), *Gneiss Domes in Orogeny*. Geological Society of America Special Paper, Boulder, Colorado, pp. 267–294.
- Siddoway, C.S., Fanning, C.M., Kruckenberg, S.C., Fadrhonc, S.C., 2006. U–Pb SHRIMP investigation of the timing and duration of melt production and migration in a Pacific margin gneiss dome, Fosdick Mountains, Antarctica. *Eos Trans. AGU*, vol. 87, V23D-0661.
- Siddoway, C.S., McFadden, R., Teyssier, C., Fanning, C.M., Vail, R., 2008. Characterization of melt-transfer to accumulation in a transcurrent zone using U–Pb SHRIMP geochronology, meso- and microstructures of granites, Fosdick Mountains, Antarctica. *Geological Association of Canada – Mineralogical Association of Canada, Quebec Abstracts* 33, 158–159.
- Spaggiari, C.V., Gray, D.R., Foster, D.A., Fanning, C.M., 2002. Occurrence and significance of blueschist in the southern Lachlan Orogen. *Australian Journal of Earth Sciences* 49, 255–269.
- Spaggiari, C.V., Gray, D.R., Foster, D.A., McKnight, S., 2003. Evolution of the boundary between the western and central Lachlan Orogen: implications for Tasmanide tectonics. *Australian Journal of Earth Sciences* 50, 725–749.
- Tera, F., Wasserburg, G., 1972. U–Th–Pb systematics in three Apollo 14 basalts and the problem of initial Pb in lunar rocks. *Earth and Planetary Science Letters* 14, 281–304. doi:10.1016/0012-821X(72)90128-8.
- Tulloch, A.J., Ramezani, J., Kimbrough, D.L., Faure, K., Allibone, A.H., 2009. U–Pb geochronology of Paleozoic plutonism in western New Zealand: Implications for S-type granite generation and growth of the East Gondwana margin. *Geological Society of America Bulletin* 121, 1236–1261.
- VandenBerg, A.H.M., Williman, C.E., Maher, S., Simons, B.A., Cayley, R.A., Taylor, D.H., Morand, V.J., Moore, D.H., Radojkovic, A., 2000. The Tasman Fold Belt system in Victoria: geology and mineralisation of Proterozoic to Carboniferous rocks. *Geological Survey of Victoria Special Publication*, 462 pp.
- Weaver, S.D., Bradshaw, J.D., Adams, C.J., 1991. Granitoids of the Ford Ranges, Marie Byrd Land, Antarctica. In: Thomson, M.R.A., Crame, J.A., Thomson, J.W. (Eds.), *Geological Evolution of Antarctica*. Cambridge University Press, Cambridge, pp. 345–351.
- Williams, I.S., 1998. U–Th–Pb geochronology by ion microprobe. In: McKibben, M.A., Shanks III, W.C., Ridley, W.J. (Eds.), *Application of Microanalytical Techniques to Understanding Mineralizing Processes*. Reviews in Economic Geology. Society of Economic Geologists, Littleton, CO, pp. 1–35.
- Williams, I.S., Claesson, S., 1987. Isotopic evidence for the Precambrian provenance and Caledonian metamorphism of high grade paragneisses from the Seve Nappes, Scandinavian Caledonides. II. Ion microprobe zircon U–Th–Pb. *Contributions to Mineralogy and Petrology* 97, 205–217.